Robotica (2024), **42**, pp. 510–535
doi:10.1017/S0263574723001601

CAMBRIDGE UNIVERSITY PRESS

RESEARCH ARTICLE

Hybrid impedance and admittance control for optimal robot–environment interaction

Dexi Ye[1], Chenguang Yang[1], Yiming Jiang[2] and Hui Zhang[2]

[1]Key Laboratory of Autonomous Systems and Networked Control, School of Automation Science and Engineering, South China University of Technology, Guangzhou, 510640, China and [2]School of Robotics and the Visual Perception and Control Technology National Engineering Laboratory, Hunan University, Changsha, 410082, China
Corresponding author: Chenguang Yang; Email: cyang@ieee.org

Received: 17 May 2023; **Revised:** 31 October 2023; **Accepted:** 31 October 2023; **First published online:** 30 November 2023

Keywords: impedance control; impedance adaptation; admittance control; optimal control; hybrid system

Abstract

Compliant interaction between robots and the environment is crucial for completing contact-rich tasks. However, obtaining and implementing optimal interaction behavior in complex unknown environments remains a challenge. This article develops a hybrid impedance and admittance control (HIAC) scheme for robots subjected to the second-order unknown environment. To obtain the second-order target impedance model that represents the optimal interaction behavior without the accurate environment dynamics and acceleration feedback, an impedance adaptation method with virtual inertia is proposed. Since impedance control and admittance control have complementary structures and result in unsatisfactory performance in a wide range of environmental stiffness due to their fixed causality, a hybrid system framework suitable for the second-order environment is proposed to generate a series of intermediate controllers which interpolate between the responses of impedance and admittance controls by using a switching controller and adjusting its switching duty cycle. In addition, the optimal intermediate controller is selected using a mapping of the optimal duty cycle to provide the optimal implementation performance for the target impedance model. The proposed HIAC scheme can achieve the desired interaction and impedance implementation performance while ensuring system stability. Simulation and experimental studies are performed to verify the effectiveness of our scheme with a 2-DOF manipulator and a 7-DOF Franka EMIKA panda robot, respectively.

1. Introduction

With the rapid increase of robots landing in various fields, robots inevitably interact with the external environment in contact-rich applications such as assembly automation and human–robot collaboration [1, 2]. However, the environment is usually unknown and uncertain in these scenarios, making it quite challenging to ensure safe and effective interactions during the tasks. In the existing research, two methods have been widely used to achieve compliant interaction behaviors between manipulators and the environment. The first method is hybrid position/force control proposed by Raibert and Craig [3], which decomposes the task space into position-controlled and force-controlled subspaces but will easily result in the instability of the interaction when the modeling accuracy of the environment or robot dynamics is insufficient. The second method is impedance control proposed by Hogan [4], whose goal is to establish a dynamical relationship between the motion of the manipulator and the interaction force, rather than controlling these variables separately. Moreover, impedance control has proven to be easier to implement and more robust [5].

In impedance control, obtaining the target impedance model which describes the desired interaction behavior is necessary. A basic approach is to impose a passive impedance model on the manipulator, which can guarantee the interaction stability under any passive environment [6]. Further, the environment dynamics were considered since the model's passivity cannot guarantee that the

© The Author(s), 2023. Published by Cambridge University Press.

https://doi.org/10.1017/S0263574723001601 Published online by Cambridge University Press

manipulator can adapt to the environment [7]. The adaptive impedance controllers using polynomial universal approximators and q-Chlodowsky operators to approximate the system uncertainties, unmodeled dynamics, and external disturbances were designed in refs. [8, 9]. However, obtaining an impedance model that matches the environment is difficult since the environment dynamics are usually unknown. Moreover, a fixed target impedance model is not applicable in many flexible tasks such as human–robot collaboration [10, 11], so a variable admittance control approach was proposed by ref. [12] to tune the inertia and provide the robot with the adaptive ability to cope with different task states in human–robot cooperation. In ref. [13], a sensorless optimal switching impact/force controller with impedance adaptive mechanism was proposed to realize stable free-space/contact phase control of the robot. In ref. [14], a sensorless model-based method was proposed to estimate the environmental stiffness and tune impedance gains online. A Q-Learning-based model predictive variable impedance controller was developed, which can learn the human–robot interaction dynamics and uncertainties and optimize the impedance parameters [15]. Therefore, iterative learning was utilized to update the impedance parameters iteratively through repeated contact operations of the manipulator, leading to the desired impedance model adapted to the unknown environment [16]. The reference adaptation approach was used to parameterize the desired trajectory and iteratively search for the optimal parameter to obtain the desired interaction performance [17]. However, the repeated operations in iterative learning are inflexible and time-consuming, so the impedance adaptation which has the potential to obviate the repeated operations of the manipulator has been focused on. In ref. [18], a bioinspired approach derived from human motor learning was proposed to adapt the impedance and feedforward torque in the unknown and dynamic environment to meet the requirements of interaction. In ref. [19], the advanced research on human-inspired intelligent robots was summarized and a significant insight into the principle of human-like impedance adaptation for robots was provided. Further, a brain-inspired intelligent robotic system was established in ref. [20], which strongly proved the effectiveness of human-like impedance adaptation for improving the performance of robots.

In general, the target impedance model discussed above corresponds to a good trade-off between trajectory tracking and interaction force regulation obtained by optimization. When the environment dynamics are known, the optimal impedance parameters can be easily obtained using the well-known linear quadratic regulator (LQR). However, LQR is not suitable for unknown linear systems caused by unknown environment dynamics [21]. Hence, adaptive dynamic programming (ADP), as a method to design the optimal controller with only partial information of the controlled system model, has attracted wide attention [22]. Based on the ADP approach in ref. [23], an impedance adaptation method was proposed to obtain the target impedance parameters that guarantee the optimal interaction in the unknown environment without repeated operations of the manipulator [24]. As an improvement of ref. [24], an auxiliary function was designed in the impedance adaptation to make the feedback gain change smoothly, and the broad fuzzy neural network and the barrier Lyapunov function were used to deal with the uncertainty of robot dynamics and the state constraint problem [25]. In ref. [26], an admittance adaptation method was proposed for the unknown environment, where a torque observer was employed and an advanced adaptive controller was designed to ensure trajectory tracking performance. However, in the second-order environment, namely the mass–spring–damper environment, the methods in refs. [24–26] can only obtain a first-order target impedance model, namely spring–damper model, which has a limited range to describe the interaction behavior and thus is not suitable for many tasks.

In practice, not only the acquisition of the target impedance model but also its implementation should be considered carefully, both of which ensure the desired interaction behavior of the manipulator interacting with the environment. According to the different causality, impedance control can be implemented in two ways, which are referred to as "impedance control" and "admittance control." In essence, these two controllers have complementary stability and performance due to their fixed causality [27, 28], which is qualitatively shown in Fig. 1. To be specific, due to the inability of impedance control to provide stiff behavior, impedance control results in poor position accuracy in free motion and soft environments affected by uncompensated frictions, but it can guarantee stability and provide good performance in interaction with stiff environments. On the contrary, admittance control results in poor robustness and

https://doi.org/10.1017/S0263574723001601 Published online by Cambridge University Press

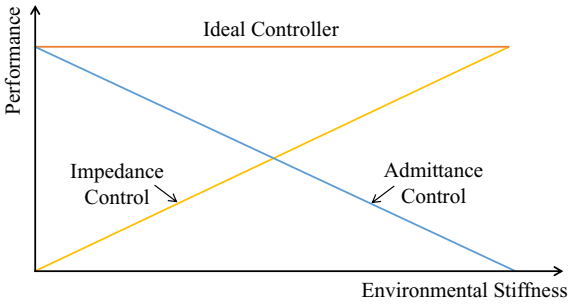

Figure 1. *Qualitative representation of impedance and admittance controllers performance. Neither of these two controllers is well adapted to a wide range of environmental stiffness, so it is necessary to design an ideal controller that can provide good performance in any environment stiffness [28].*

even instability in stiff environments due to its stiff characteristic but can compensate for unmodeled frictions and provide high position accuracy in free motion and soft environments.

To cope with this problem, Ott, Mukherjee, and Nakamura proposed a hybrid system framework to achieve the performance of the ideal controller in Fig. 1 [28, 29]. By utilizing the switching controller according to the switching period and duty cycle, the framework interpolates between the responses of impedance control and admittance control and provides good performance in a wide range of environmental stiffness. As an improvement of ref. [29], a hybrid controller that can adapt the switching period and duty cycle was developed to improve the control performance [30]. In ref. [31], a hybrid control strategy was proposed, where the switch between impedance and admittance controllers was triggered by the position error, which led to good performance under any impedance condition. To obtain the optimal implementation performance of the target impedance model in different environments, an adaptive hybrid system framework was proposed by ref. [32] using the neural network based on ref. [29], which directly established the mapping of the states and force of the robot to the optimal duty cycle to obtain the intermediate controller that provided the optimal performance in a fixed or time-varying environment. It is worth noting that although environmental stiffness is the main factor affecting the performance of impedance and admittance controllers, environmental inertia and damping in the second-order environment also need to be considered since they greatly affect the system stability. However, the above approaches consider neither the acquisition of the optimal impedance model nor the interaction with the second-order environment.

According to the above discussion, this article proposes a hybrid impedance and admittance control (HIAC) scheme to address two problems. The first problem is that existing impedance adaptation methods [24–26] can only obtain insufficient first-order impedance models in the second-order unknown environment. The second problem is that existing hybrid control methods [28–32] do not consider the interaction with the second-order environment. Therefore, this inspires us to propose a unified scheme to optimally obtain and implement the target impedance model for the manipulator subjected to the second-order unknown environment. It should be noted that although the uncertainties and environment dynamics lead to differences in the performance of impedance control and admittance control due to their different causality, our goal is not to compensate for system uncertainties like conventional adaptive impedance control but to utilize the hybrid system framework to provide optimal consistent impedance implementation performance independent of the environmental stiffness under unknown uncertainties and the second-order environment. Compared with the existing research, the main contributions of this article are summarized below:

1. An impedance adaptation method with virtual inertia is proposed to obtain the second-order target impedance model representing the optimal interaction behavior in the second-order unknown environment without the accurate environment dynamics and acceleration feedback.

https://doi.org/10.1017/S0263574723001601 Published online by Cambridge University Press

2. A hybrid system framework suitable for the second-order environment is proposed to implement the target impedance model with its stability analyzed.
3. A mapping of the optimal duty cycle is built to select the optimal intermediate controller to provide the optimal implementation performance for the obtained target impedance model.

The rest of this article is organized as follows. In Section 2, the preliminaries including the robot and environment dynamics, LQR, and impedance control and admittance control are introduced. Section 3 introduces the methodologies containing the adaptive optimal control, impedance adaptation, and hybrid system framework with its stability analysis and mapping of the optimal duty cycle. Simulation and experimental studies are conducted in Section 4 and 5 to verify the effectiveness of the proposed HIAC scheme, respectively. Section 6 gives the conclusions.

2. Preliminaries

2.1. System model

For the system, we consider that an n-DOF rigid robot manipulator is in interaction with an environment. The forward kinematics of the manipulator is given first:

$$\boldsymbol{x} = \phi(\boldsymbol{q}) \tag{1}$$

where $\boldsymbol{x}$ and $\boldsymbol{q} \in \mathbb{R}^n$ denote the end-effector's coordinates in Cartesian space and joint angle vector in joint space, respectively. Differentiating (1) along time yields

$$\dot{\boldsymbol{x}} = \boldsymbol{J}(\boldsymbol{q})\dot{\boldsymbol{q}} \tag{2}$$

where $\boldsymbol{J}(\boldsymbol{q})$ is the Jacobian matrix. Differentiating (2) along time, we have

$$\ddot{\boldsymbol{x}} = \dot{\boldsymbol{J}}(\boldsymbol{q})\dot{\boldsymbol{q}} + \boldsymbol{J}(\boldsymbol{q})\ddot{\boldsymbol{q}}. \tag{3}$$

The nominal dynamics of the robot manipulator without considering the uncertainties and frictions in joint space are given by ref. [18]:

$$\boldsymbol{H}(\boldsymbol{q})\ddot{\boldsymbol{q}} + \boldsymbol{C}(\boldsymbol{q}, \dot{\boldsymbol{q}})\dot{\boldsymbol{q}} + \boldsymbol{G}(\boldsymbol{q}) = \boldsymbol{\tau}_c + \boldsymbol{J}^T(\boldsymbol{q})\boldsymbol{F}_e \tag{4}$$

where $\boldsymbol{H}(\boldsymbol{q}) \in \mathbb{R}^{n\times n}$ is the inertia matrix. $\boldsymbol{C}(\boldsymbol{q}, \dot{\boldsymbol{q}})\dot{\boldsymbol{q}} \in \mathbb{R}^n$ is the Coriolis and Centrifugal force vector. $\boldsymbol{G}(\boldsymbol{q}) \in \mathbb{R}^n$ is the gravitational force vector. $\boldsymbol{\tau}_c \in \mathbb{R}^n$ is the control torque input vector, and $\boldsymbol{F}_e \in \mathbb{R}^n$ denotes the force applied by the external environment. Since the interaction is conducted in Cartesian space, the robot dynamics in joint space is transformed to Cartesian space to simplify the analysis. Integrating (2) and (3) into (4), the nominal robot dynamics in Cartesian space can be described by:

$$\boldsymbol{H}_x(\boldsymbol{q})\ddot{\boldsymbol{x}} + \boldsymbol{C}_x(\boldsymbol{q}, \dot{\boldsymbol{q}})\dot{\boldsymbol{x}} + \boldsymbol{G}_x(\boldsymbol{q}) = \boldsymbol{F}_c + \boldsymbol{F}_e \tag{5}$$

where

$$\begin{aligned}
\boldsymbol{H}_x(\boldsymbol{q}) &= \boldsymbol{J}^{-T}(\boldsymbol{q})\boldsymbol{H}(\boldsymbol{q})\boldsymbol{J}^{-1}(\boldsymbol{q}),\\
\boldsymbol{C}_x(\boldsymbol{q}, \dot{\boldsymbol{q}}) &= \boldsymbol{J}^{-T}(\boldsymbol{q})(\boldsymbol{C}(\boldsymbol{q}, \dot{\boldsymbol{q}}) - \boldsymbol{H}(\boldsymbol{q})\boldsymbol{J}^{-1}(\boldsymbol{q})\dot{\boldsymbol{J}}(\boldsymbol{q}))\boldsymbol{J}^{-1}(\boldsymbol{q}),\\
\boldsymbol{G}_x(\boldsymbol{q}) &= \boldsymbol{J}^{-T}(\boldsymbol{q})\boldsymbol{G}(\boldsymbol{q})
\end{aligned}$$

and $\boldsymbol{F}_c = \boldsymbol{J}^{-T}(\boldsymbol{q})\boldsymbol{\tau}_c$ denotes the control force input vector. To proceed, we consider the environment model. Without the loss of generality, the environment dynamics can be described by a mass–spring–damper system as below [24]:

$$\boldsymbol{H}_m\ddot{\boldsymbol{x}} + \boldsymbol{C}_m\dot{\boldsymbol{x}} + \boldsymbol{G}_m\boldsymbol{x} = -\boldsymbol{F}_e \tag{6}$$

where $\boldsymbol{H}_m$, $\boldsymbol{C}_m$, and $\boldsymbol{G}_m$ are unknown environmental inertia, damping, and stiffness matrices, respectively. A typical mass–spring–damper environment model is shown in Fig. 2.

https://doi.org/10.1017/S0263574723001601 Published online by Cambridge University Press

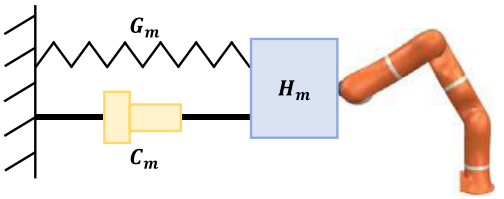

Figure 2. *Model of the mass–spring–damper environment.*

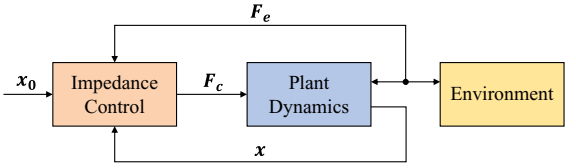

Figure 3. *Diagram of impedance control.*

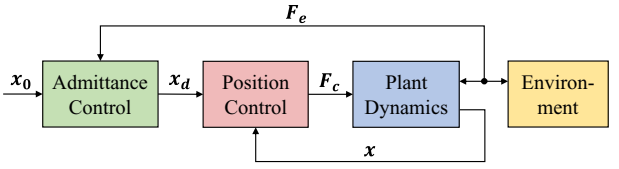

Figure 4. *Diagram of admittance control.*

Remark 1. As a second-order system, the mass–spring–damper model can describe a wider range of environments than the damper–spring model. For example, (6) can describe the environment dynamics in human–robot interaction. To simplify the analysis, the environmental inertia, damping, and stiffness are assumed to be fixed.

2.2. Impedance control and admittance control

Impedance control and admittance control are two complementary implementations of regulating the mechanical impedance of manipulators to the target impedance model described by:

$$\boldsymbol{F}_e = f(\boldsymbol{x}, \boldsymbol{x}_0) \tag{7}$$

where $\boldsymbol{x}_0$ is the virtual equilibrium trajectory and $f(\cdot)$ is a target impedance function. Equation (7) is a general impedance model which describes a dynamical relationship between the motion and the contact force. In this article, we adopt the impedance model $\boldsymbol{F}_e = \boldsymbol{H}_d\ddot{\boldsymbol{x}} + \boldsymbol{C}_d\dot{\boldsymbol{x}} + \boldsymbol{K}_d\boldsymbol{x} - \boldsymbol{K}_d'\boldsymbol{x}_0$ as the target, where $\boldsymbol{H}_d$, $\boldsymbol{C}_d$, $\boldsymbol{K}_d$, and $\boldsymbol{K}_d'$ are the desired inertia, damping, stiffness, and auxiliary stiffness matrices, respectively.

In impedance control, as the controlled plant, robot dynamics (5) acts as an admittance, so the controller is designed as an impedance accordingly. The control force $\boldsymbol{F}_c$ is designed to eliminate the difference between the robot dynamics and the target impedance model directly. While in admittance control, an outer loop controller and an inner loop controller need to be designed. The outer loop controller generates the desired trajectory $\boldsymbol{x}_d$ that satisfies the desired interaction behavior. By replacing $\boldsymbol{x}$ with $\boldsymbol{x}_d$ in (7), the form of the outer loop controller becomes $\boldsymbol{F}_e = f(\boldsymbol{x}_d, \boldsymbol{x}_0)$. The inner loop controller ensures trajectory tracking, that is, $\lim_{t\to\infty} \boldsymbol{x}(t) = \boldsymbol{x}_d(t)$. On the contrary, admittance control regards the position-controlled system including the inner loop controller as the controlled plant, which acts as an impedance, so the outer loop controller is designed as an admittance. The diagrams of these two controllers are illustrated in Fig. 3 and Fig. 4, respectively.

https://doi.org/10.1017/S0263574723001601 Published online by Cambridge University Press

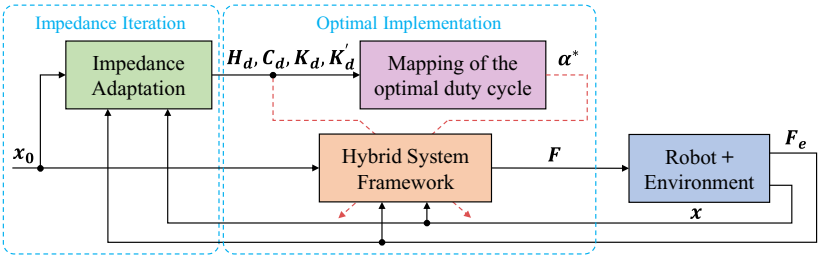

Figure 5. *Diagram of HIAC scheme.*

2.3. LQR

Consider a continuous linear time-invariant system described by:

$$\dot{\boldsymbol{\xi}} = \boldsymbol{A}\boldsymbol{\xi} + \boldsymbol{B}\boldsymbol{u} \tag{8}$$

where $\boldsymbol{\xi} \in \mathbb{R}^m$ and $\boldsymbol{u} \in \mathbb{R}^r$ denote the system state and input, respectively. $\boldsymbol{A} \in \mathbb{R}^{m\times m}$ and $\boldsymbol{B} \in \mathbb{R}^{m\times r}$ denote the system matrix and input matrix, respectively. The goal is to design the optimal control input:

$$\boldsymbol{u} = -\boldsymbol{K}\boldsymbol{\xi} \tag{9}$$

to minimize the cost function:

$$J = \int_0^\infty \left(\boldsymbol{\xi}^T \boldsymbol{Q}\boldsymbol{\xi} + \boldsymbol{u}^T \boldsymbol{R}\boldsymbol{u}\right) dt \tag{10}$$

where $\boldsymbol{Q} \in \mathbb{R}^{m\times m}$ and $\boldsymbol{R} \in \mathbb{R}^{r\times r}$ denote the weights of system state and input satisfying $\boldsymbol{Q} = \boldsymbol{Q}^T \geq \boldsymbol{0}$ and $\boldsymbol{R} = \boldsymbol{R}^T > \boldsymbol{0}$. By solving the algebraic Riccati equation (ARE) using known $\boldsymbol{A}$ and $\boldsymbol{B}$, the unique symmetric positive definite matrix $\boldsymbol{Y}^*$ can be obtained [21]:

$$\boldsymbol{Y}\boldsymbol{A} + \boldsymbol{A}^T\boldsymbol{Y} + \boldsymbol{Q} - \boldsymbol{Y}\boldsymbol{B}\boldsymbol{R}^{-1}\boldsymbol{B}^T\boldsymbol{Y} = \boldsymbol{0}. \tag{11}$$

Then, we can calculate the optimal feedback gain $\boldsymbol{K}^*$ in (9):

$$\boldsymbol{K}^* = \boldsymbol{R}^{-1}\boldsymbol{B}^T\boldsymbol{Y}^*. \tag{12}$$

3. Methodology

In this section, the HIAC scheme under the second-order unknown environment is illustrated, which can be divided into the impedance iteration stage and optimal implementation stage, as shown in Fig. 5. In the impedance iteration stage, the target impedance model is adjusted iteratively by the proposed impedance adaptation method to minimize the cost function. In the optimal implementation stage, the obtained target impedance model is implemented optimally by the proposed hybrid system framework with the mapping of the optimal duty cycle.

3.1. Adaptive optimal control

In this section, an adaptive optimal control method is to solve the optimal feedback gain that minimizes the cost function (10) when $\boldsymbol{A}$ and $\boldsymbol{B}$ in the system (8) are unknown constant matrices [23]. The required definitions are first imported as:

https://doi.org/10.1017/S0263574723001601 Published online by Cambridge University Press

$$\begin{aligned}
\hat{\boldsymbol{Y}} &= [Y_{11}, 2Y_{12}, \cdots, 2Y_{1m}, Y_{22}, 2Y_{23}, \cdots, Y_{mm}]^T \\
\bar{\boldsymbol{\xi}} &= \left[\xi_1^2, \xi_1\xi_2, \cdots, \xi_1\xi_m, \xi_2^2, \xi_2\xi_3, \cdots, \xi_m^2\right]^T \\
\boldsymbol{\delta}_{\xi\xi} &= \left[\bar{\boldsymbol{\xi}}(t_1) - \bar{\boldsymbol{\xi}}(t_0), \bar{\boldsymbol{\xi}}(t_2) - \bar{\boldsymbol{\xi}}(t_1), \cdots, \bar{\boldsymbol{\xi}}(t_l) - \bar{\boldsymbol{\xi}}(t_{l-1})\right]^T \\
\boldsymbol{I}_{\xi\xi} &= \left[\int_{t_0}^{t_1} \boldsymbol{\xi} \otimes \boldsymbol{\xi} dt, \int_{t_1}^{t_2} \boldsymbol{\xi} \otimes \boldsymbol{\xi} dt, \cdots, \int_{t_{l-1}}^{t_l} \boldsymbol{\xi} \otimes \boldsymbol{\xi} dt\right]^T \\
\boldsymbol{I}_{\xi u} &= \left[\int_{t_0}^{t_1} \boldsymbol{\xi} \otimes \boldsymbol{u} dt, \int_{t_1}^{t_2} \boldsymbol{\xi} \otimes \boldsymbol{u} dt, \cdots, \int_{t_{l-1}}^{t_l} \boldsymbol{\xi} \otimes \boldsymbol{u} dt\right]^T
\end{aligned} \tag{13}$$

where $0 \le t_0 < t_1 < \cdots < t_l$, $\boldsymbol{Y} \in \mathbb{R}^{m\times m} \to \hat{\boldsymbol{Y}} \in \mathbb{R}^{\frac{1}{2}m(m+1)}$, $\boldsymbol{\xi} \in \mathbb{R}^m \to \bar{\boldsymbol{\xi}} \in \mathbb{R}^{\frac{1}{2}m(m+1)}$, $\boldsymbol{\delta}_{\xi\xi} \in \mathbb{R}^{l\times\frac{1}{2}m(m+1)}$, $\boldsymbol{I}_{\xi\xi} \in \mathbb{R}^{l\times m^2}$, $\boldsymbol{I}_{\xi u} \in \mathbb{R}^{l\times mr}$, $\boldsymbol{P}_{ij}$ and ξ_i denote the elements of $\boldsymbol{Y}$ and $\boldsymbol{\xi}$, respectively, l is the sampling times, and $\otimes$ is the Kronecker product.

The initial system input of time interval $t \in [t_0, t_l]$ is designed as $\boldsymbol{u} = -\boldsymbol{K_0}\boldsymbol{\xi} + \boldsymbol{v}$, where $\boldsymbol{K_0}$ is the initial feedback gain to stabilize the system and $\boldsymbol{v}$ is the exploration noise to make the system satisfy the persistent excitation (PE) condition. The matrices $\boldsymbol{\delta}_{\xi\xi}$, $\boldsymbol{I}_{\xi\xi}$, and $\boldsymbol{I}_{\xi u}$ defined above are computed until the rank condition is satisfied:

$$\operatorname{rank}\left([\boldsymbol{I}_{\xi\xi}, \boldsymbol{I}_{\xi u}]\right) = \frac{1}{2}m(m+1) + mr. \tag{14}$$

When the sampling times l is large enough and the rank condition (14) is satisfied, $\boldsymbol{Y_k}$ and $\boldsymbol{K_{k+1}}$ can be computed iteratively by:

$$\begin{bmatrix} \hat{\boldsymbol{Y}}_k \\ \operatorname{vec}(\boldsymbol{K_{k+1}}) \end{bmatrix} = \left(\boldsymbol{\Theta}_k^T \boldsymbol{\Theta}_k\right)^{-1} \boldsymbol{\Theta}_k^T \boldsymbol{\Xi}_k \tag{15}$$

where k is the number of iterations. $\boldsymbol{\Theta_k}$ and $\boldsymbol{\Xi_k}$ are defined as:

$$\begin{aligned}
\boldsymbol{\Theta}_k &= \left[\boldsymbol{\delta}_{\xi\xi}, -2\boldsymbol{I}_{\xi\xi}\left(\boldsymbol{I}_m \otimes \boldsymbol{K}_k^T\boldsymbol{R}\right) - 2\boldsymbol{I}_{\xi u}(\boldsymbol{I}_m \otimes \boldsymbol{R})\right] \\
\boldsymbol{\Xi}_k &= -\boldsymbol{I}_{\xi\xi}\operatorname{vec}\left(\boldsymbol{Q} + \boldsymbol{K}_k^T\boldsymbol{R}\boldsymbol{K}_k\right)
\end{aligned} \tag{16}$$

where $\boldsymbol{I_m} \in \mathbb{R}^{m\times m}$ is an identity matrix and $\operatorname{vec}(\cdot)$ is the function that stretches a matrix into a vector. Let $k+1 \to k$ and repeat the above calculation until $\|\boldsymbol{Y_k} - \boldsymbol{Y_{k-1}}\| \le \varepsilon$ where $\varepsilon > 0$ is a preset threshold, and the optimal feedback gain $\boldsymbol{K_k}$ is obtained. To proceed, we design smooth functions for the feedback gain and the exploration noise to keep the system input continuous [25]:

$$\begin{aligned}
\boldsymbol{K}_k' &= \frac{\boldsymbol{K_k} + \boldsymbol{K_0}}{2} + \frac{\boldsymbol{K_k} - \boldsymbol{K_0}}{2}\sin\left(-\frac{\pi}{2} + \frac{t - t_l}{T_s}\pi\right) \\
\boldsymbol{v}' &= \frac{\boldsymbol{v}(t_l)}{2} - \frac{\boldsymbol{v}(t_l)}{2}\sin\left(-\frac{\pi}{2} + \frac{t - t_l}{T_s}\pi\right)
\end{aligned} \tag{17}$$

where $\boldsymbol{K}_k'$ is the transitional feedback gain, $\boldsymbol{v}'$ is the transitional exploration noise, $\boldsymbol{v}(t_l)$ is the value of $\boldsymbol{v}$ at time t_l, and T_s is the transitional time. The transitional system input is designed as $\boldsymbol{u} = -\boldsymbol{K}_k'\boldsymbol{\xi} + \boldsymbol{v}'$ in time interval $t_l < t \le t_l + T_s$ during which $\boldsymbol{K}_k'$ changes from $\boldsymbol{K_0}$ to $\boldsymbol{K_k}$ and $\boldsymbol{v}'$ changes from $\boldsymbol{v}(t_l)$ to $\boldsymbol{0}$ smoothly. When $t > t_l + T_s$, the system input becomes $\boldsymbol{u} = -\boldsymbol{K_k}\boldsymbol{\xi}$. The principle of the above algorithm is summarized in Algorithm 1.

3.2. Impedance adaptation

In this section, we propose a novel impedance adaptation method to obtain the optimal second-order target impedance model in the second-order unknown environment. Assume that the manipulator is interacting with a virtual environment that consists of two parts, one is the mass–spring–damper system

https://doi.org/10.1017/S0263574723001601 Published online by Cambridge University Press

Algorithm 1. Adaptive Optimal Control

Input: Initial feedback gain $\boldsymbol{K_0}$, exploration noise $\boldsymbol{\nu}$, state variable $\boldsymbol{\xi}$, preset threshold ε;
Output: Optimal feedback gain $\boldsymbol{K_k}$;
repeat
  Set the initial system input as $\boldsymbol{u} = -\boldsymbol{K_0}\boldsymbol{\xi} + \boldsymbol{\nu}$;
  Compute $\boldsymbol{\delta_{\xi\xi}}$, $\boldsymbol{I_{\xi\xi}}$ and $\boldsymbol{I_{\xi u}}$;
until $\mathrm{rank}([\boldsymbol{I_{\xi\xi}}, \boldsymbol{I_{\xi u}}]) = \frac{1}{2}m(m+1) + mr$;
repeat
  Solve $\boldsymbol{Y_k}$ and $\boldsymbol{K_{k+1}}$ in (15);
  Let $k+1 \rightarrow k$;
until $\|\boldsymbol{Y_k} - \boldsymbol{Y_{k-1}}\| \leq \varepsilon$;
repeat
  Set the transitional system input as $\boldsymbol{u} = -\boldsymbol{K_k'}\boldsymbol{\xi} + \boldsymbol{\nu'}$;
  Calculate $\boldsymbol{K_k'}$ and $\boldsymbol{\nu'}$ in (17);
until $t > t_l + T_s$;
return $\boldsymbol{K_k}$;

described in (6) and the other is the virtual inertia denoted as $\boldsymbol{H_d}$, which is realized by defining the virtual interaction force $\boldsymbol{F_{ev}}$ as:

$$\boldsymbol{F_{ev}} = \boldsymbol{F_e} - \boldsymbol{H_d}\ddot{\boldsymbol{x}}. \tag{18}$$

Substituting (18) into (6), we have

$$\boldsymbol{H_t}\ddot{\boldsymbol{x}} + \boldsymbol{C_m}\dot{\boldsymbol{x}} + \boldsymbol{G_m}\boldsymbol{x} = -\boldsymbol{F_{ev}} \tag{19}$$

where $\boldsymbol{H_t} = \boldsymbol{H_m} + \boldsymbol{H_d}$ denotes the total inertia of the virtual environment. Compare (8) with (19), we need to rewrite (19) as a linear time-invariant system [24]:

$$\dot{\boldsymbol{\xi}} = \boldsymbol{A}\boldsymbol{\xi} + \boldsymbol{B}\boldsymbol{F_{ev}} \tag{20}$$

where $\boldsymbol{\xi} = [\dot{\boldsymbol{x}}^T, \boldsymbol{x}^T, \boldsymbol{z}^T]^T$ is the system state and $\boldsymbol{z} \in \mathbb{R}^p$ is generated by:

$$\begin{cases} \dot{\boldsymbol{z}} = \boldsymbol{U}\boldsymbol{z} \\ \boldsymbol{x_0} = \boldsymbol{V}\boldsymbol{z} \end{cases} \tag{21}$$

where $\boldsymbol{U} \in \mathbb{R}^{p\times p}$ and $\boldsymbol{V} \in \mathbb{R}^{n\times p}$ are two predefined matrices. Then, we have

$$\boldsymbol{A} = \begin{bmatrix} -\boldsymbol{H_t}^{-1}\boldsymbol{C_m} & -\boldsymbol{H_t}^{-1}\boldsymbol{G_m} & \boldsymbol{0} \\ \boldsymbol{I_n} & \boldsymbol{0} & \boldsymbol{0} \\ \boldsymbol{0} & \boldsymbol{0} & \boldsymbol{U} \end{bmatrix}, \boldsymbol{B} = \begin{bmatrix} -\boldsymbol{H_t}^{-1} \\ \boldsymbol{0} \\ \boldsymbol{0} \end{bmatrix} \tag{22}$$

where $\boldsymbol{A}$ and $\boldsymbol{B}$ are unknown due to the unknown environment dynamics. A cost function that represents the trade-off between trajectory tracking and force regulation is defined as:

$$J_1 = \int_0^\infty \left[\dot{\boldsymbol{x}}^T\boldsymbol{Q_1}\dot{\boldsymbol{x}} + (\boldsymbol{x} - \boldsymbol{x_0})^T\boldsymbol{Q_2}(\boldsymbol{x} - \boldsymbol{x_0}) + \boldsymbol{F_{ev}^T}\boldsymbol{R}\boldsymbol{F_{ev}}\right]dt \tag{23}$$

where $\boldsymbol{Q_1}, \boldsymbol{Q_2} \in \mathbb{R}^{n\times n}$ are the weights of tracking error and $\boldsymbol{R} \in \mathbb{R}^{n\times n}$ is the weight of the virtual interaction force. According to the states defined above, (23) can be rewritten as:

$$J_1 = \int_0^\infty \left(\boldsymbol{\xi}^T\boldsymbol{Q}\boldsymbol{\xi} + \boldsymbol{F_{ev}^T}\boldsymbol{R}\boldsymbol{F_{ev}}\right)dt \tag{24}$$

https://doi.org/10.1017/S0263574723001601 Published online by Cambridge University Press

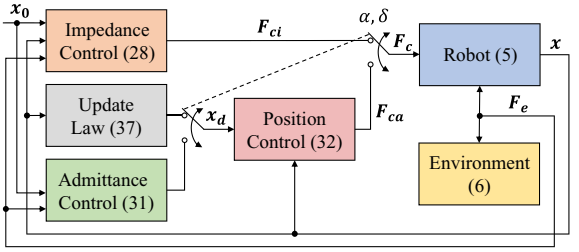

Figure 6. *Diagram of hybrid system framework.*

where

$$\boldsymbol{Q} = \begin{bmatrix} \boldsymbol{Q}_1 & \boldsymbol{0} & \boldsymbol{0} \\ \boldsymbol{0} & \boldsymbol{Q}_2 & -\boldsymbol{Q}_2\boldsymbol{V} \\ \boldsymbol{0} & -\boldsymbol{V}^T\boldsymbol{Q}_2 & \boldsymbol{V}^T\boldsymbol{Q}_2\boldsymbol{V} \end{bmatrix}.$$

Therefore, the cost function (24) can be minimized by regarding the virtual interaction force $\boldsymbol{F}_{ev}$ in (20) as the system input:

$$\boldsymbol{F}_{ev} = -\boldsymbol{K}_k\boldsymbol{\xi} \tag{25}$$

where $\boldsymbol{K}_k = [\boldsymbol{K}_{k1}, \boldsymbol{K}_{k2}, \boldsymbol{K}_{k3}]$ is obtained according to Algorithm 1 with $\boldsymbol{K}_{k1}, \boldsymbol{K}_{k2} \in \mathbb{R}^{n\times n}$ and $\boldsymbol{K}_{k3} \in \mathbb{R}^{n\times p}$. Substituting (18) and (21) into (25), we have

$$\boldsymbol{F}_e = \boldsymbol{H}_d\ddot{\boldsymbol{x}} - \boldsymbol{K}_{k1}\dot{\boldsymbol{x}} - \boldsymbol{K}_{k2}\boldsymbol{x} - \boldsymbol{K}_{k3}\left(\boldsymbol{V}^T\boldsymbol{V}\right)^{-1}\boldsymbol{V}^T\boldsymbol{x}_0. \tag{26}$$

Comparing (26) with (7), we can rewrite (26) as:

$$\boldsymbol{F}_e = \boldsymbol{H}_d\ddot{\boldsymbol{x}} + \boldsymbol{C}_d\dot{\boldsymbol{x}} + \boldsymbol{K}_d\boldsymbol{x} - \boldsymbol{K}_d'\boldsymbol{x}_0. \tag{27}$$

Note that (27) denotes the target impedance model equivalent to the system input (25) with $\boldsymbol{C}_d = -\boldsymbol{K}_{k1}$, $\boldsymbol{K}_d = -\boldsymbol{K}_{k2}$ and $\boldsymbol{K}_d' = \boldsymbol{K}_{k3}(\boldsymbol{V}^T\boldsymbol{V})^{-1}\boldsymbol{V}^T$. So the target impedance model representing the optimal interaction behavior is obtained from the interaction dynamics of the robot and the second-order unknown environment, and the model is second order due to the introduced virtual inertia $\boldsymbol{H}_d$.

Remark 2. It can be seen from (25) that the virtual inertia eliminates the acceleration term in the system input. In addition, the system input in Algorithm 1 is realized by implementing the equivalent second-order impedance model using impedance control without acceleration feedback. Hence, the proposed method does not require acceleration feedback which is difficult to obtain in practice and can adapt to a wider range of environments than the approach in ref. [24].

3.3. Hybrid system framework

In this section, we design a novel hybrid system framework to implement the target impedance model in the second-order environment. An overview of the proposed framework is shown in Fig. 6. First, the well-known computed torque control method is utilized to design the control law [33]. For impedance control, the control law is designed in Cartesian space as:

$$\boldsymbol{F}_{ci} = \boldsymbol{H}_x(\boldsymbol{q})\boldsymbol{v}_{ci} + \boldsymbol{C}_x(\boldsymbol{q}, \dot{\boldsymbol{q}})\dot{\boldsymbol{x}} + \boldsymbol{G}_x(\boldsymbol{q}) - \boldsymbol{F}_e \tag{28}$$

where $\boldsymbol{F}_{ci}$ and $\boldsymbol{v}_{ci}$ are the control force and the equivalent input of impedance control, respectively. Substituting (28) into (5), yields

$$\ddot{\boldsymbol{x}} = \boldsymbol{v}_{ci}. \tag{29}$$

https://doi.org/10.1017/S0263574723001601 Published online by Cambridge University Press

Substituting (29) into (27), we have

$$\boldsymbol{v}_{ci} = \boldsymbol{H}_d^{-1}\left(\boldsymbol{F}_e - \boldsymbol{C}_d\dot{\boldsymbol{x}} - \boldsymbol{K}_d\boldsymbol{x} + \boldsymbol{K}_d'\boldsymbol{x}_0\right). \tag{30}$$

It can be seen that impedance control uses interaction force feedback instead of acceleration feedback due to the second-order inertia term in (27). For admittance control, replacing $\boldsymbol{x}$ in (27) with the desired trajectory $\boldsymbol{x}_d$, the update law of $\boldsymbol{x}_d$ in the outer loop controller is obtained as:

$$\boldsymbol{H}_d\ddot{\boldsymbol{x}}_d + \boldsymbol{C}_d\dot{\boldsymbol{x}}_d + \boldsymbol{K}_d\boldsymbol{x}_d - \boldsymbol{K}_d'\boldsymbol{x}_0 = \boldsymbol{F}_e. \tag{31}$$

The inner loop controller is designed as:

$$\boldsymbol{F}_{ca} = \boldsymbol{H}_x(\boldsymbol{q})\boldsymbol{v}_{ca} + \boldsymbol{C}_x(\boldsymbol{q}, \dot{\boldsymbol{q}})\dot{\boldsymbol{x}} + \boldsymbol{G}_x(\boldsymbol{q}) - \boldsymbol{F}_e \tag{32}$$

where $\boldsymbol{F}_{ca}$ is the control force of admittance control and $\boldsymbol{v}_{ca}$ is the equivalent input designed as:

$$\boldsymbol{v}_{ca} = \ddot{\boldsymbol{x}}_d - \boldsymbol{L}_v(\dot{\boldsymbol{x}} - \dot{\boldsymbol{x}}_d) - \boldsymbol{L}_p(\boldsymbol{x} - \boldsymbol{x}_d) \tag{33}$$

where $\boldsymbol{L}_p$ and $\boldsymbol{L}_v$ are the positive definite gain matrices of the inner loop controller. Substituting (32) into (5), the closed-loop dynamics of admittance control can be obtained as:

$$\ddot{\boldsymbol{x}} - \ddot{\boldsymbol{x}}_d + \boldsymbol{L}_v(\dot{\boldsymbol{x}} - \dot{\boldsymbol{x}}_d) + \boldsymbol{L}_p(\boldsymbol{x} - \boldsymbol{x}_d) = \boldsymbol{0} \tag{34}$$

where $\boldsymbol{x}$ and $\dot{\boldsymbol{x}}$ converge exponentially to $\boldsymbol{x}_d$ and $\dot{\boldsymbol{x}}_d$, respectively. Equation (34) implies that the trajectory tracking of admittance control is guaranteed. Then, we can give the switching controller [29]:

$$\boldsymbol{F}_c = \begin{cases} \boldsymbol{F}_{ci}, & t_u + c\delta \le t \le t_u + (c + 1 - \alpha)\delta \\ \boldsymbol{F}_{ca}, & t_u + (c + 1 - \alpha)\delta < t < t_u + (c + 1)\delta \end{cases} \tag{35}$$

where δ is the switching period, $\alpha \in [0, 1]$ is the duty cycle, t_u is the initial time, and c is a nonnegative integer. The controller switches between impedance control and admittance control and becomes an impedance controller when $\alpha = 0$ and an admittance controller when $\alpha = 1$. Besides, when the controller switches to admittance control, $\boldsymbol{x}_d$ and $\dot{\boldsymbol{x}}_d$ need to be determined to make the control force $\boldsymbol{F}_c$ continuous. Hence, by setting $\boldsymbol{F}_{ca} = \boldsymbol{F}_{ci}$ in impedance control phase, we have

$$\boldsymbol{v}_{ca} = \boldsymbol{v}_{ci}. \tag{36}$$

Substituting (29) and (33) into (36), the update law of $\boldsymbol{x}_d$ and $\dot{\boldsymbol{x}}_d$ can be obtained as:

$$\ddot{\boldsymbol{x}}_d - \ddot{\boldsymbol{x}} + \boldsymbol{L}_v(\dot{\boldsymbol{x}}_d - \dot{\boldsymbol{x}}) + \boldsymbol{L}_p(\boldsymbol{x}_d - \boldsymbol{x}) = \boldsymbol{0}. \tag{37}$$

Although (34) and (37) have the same form, (34) indicates that $\boldsymbol{x}$ and $\dot{\boldsymbol{x}}$ converge to $\boldsymbol{x}_d$ and $\dot{\boldsymbol{x}}_d$ in admittance control phase, respectively, while (37) indicates that $\boldsymbol{x}_d$ and $\dot{\boldsymbol{x}}_d$ converge to $\boldsymbol{x}$ and $\dot{\boldsymbol{x}}$ in impedance control phase, respectively. Note that $\boldsymbol{x}_d$ and $\dot{\boldsymbol{x}}_d$ updated by (31) and (37) are continuous in the control process.

To proceed, we will give a description of the switched system. Substituting (6) into (27), we can obtain the closed-loop ideal trajectory that is defined as $\boldsymbol{x}_{ref}$:

$$\boldsymbol{H}_t\ddot{\boldsymbol{x}}_{ref} + (\boldsymbol{C}_d + \boldsymbol{C}_m)\dot{\boldsymbol{x}}_{ref} + (\boldsymbol{K}_d + \boldsymbol{G}_m)\boldsymbol{x}_{ref} = \boldsymbol{K}_d'\boldsymbol{x}_0 \tag{38}$$

where $\boldsymbol{H}_t = \boldsymbol{H}_d + \boldsymbol{H}_m$ is defined as above. For impedance control, substituting (6) and (28) into (5), the closed-loop robot–environment interaction dynamics can be obtained as:

$$\boldsymbol{H}_t\ddot{\boldsymbol{x}} + (\boldsymbol{C}_d + \boldsymbol{C}_m)\dot{\boldsymbol{x}} + (\boldsymbol{K}_d + \boldsymbol{G}_m)\boldsymbol{x} = \boldsymbol{K}_d'\boldsymbol{x}_0. \tag{39}$$

Comparing (38) with (39), yields

$$\ddot{\boldsymbol{e}} = -\boldsymbol{H}_t^{-1}(\boldsymbol{C}_d + \boldsymbol{C}_m)\dot{\boldsymbol{e}} - \boldsymbol{H}_t^{-1}(\boldsymbol{K}_d + \boldsymbol{G}_m)\boldsymbol{e} \tag{40}$$

https://doi.org/10.1017/S0263574723001601 Published online by Cambridge University Press

where $\boldsymbol{e} = \boldsymbol{x} - \boldsymbol{x}_{ref}$ is defined as the error between the actual and ideal trajectories, so we can rewrite (37) as:

$$\ddot{\boldsymbol{e}}_d - \ddot{\boldsymbol{e}} + \boldsymbol{L}_v(\dot{\boldsymbol{e}}_d - \dot{\boldsymbol{e}}) + \boldsymbol{L}_p(\boldsymbol{e}_d - \boldsymbol{e}) = \boldsymbol{0} \tag{41}$$

where $\boldsymbol{e}_d = \boldsymbol{x}_d - \boldsymbol{x}_{ref}$. Comparing (40) with (41), we have

$$\begin{aligned}\ddot{\boldsymbol{e}}_d = &- \boldsymbol{L}_v\dot{\boldsymbol{e}}_d - \boldsymbol{L}_p\boldsymbol{e}_d + \left[\boldsymbol{L}_v - \boldsymbol{H}_t^{-1}(\boldsymbol{C}_d + \boldsymbol{C}_m)\right]\dot{\boldsymbol{e}} \\ &+ [\boldsymbol{L}_p - \boldsymbol{H}_t^{-1}(\boldsymbol{K}_d + \boldsymbol{G}_m)]\boldsymbol{e}.\end{aligned} \tag{42}$$

For admittance control, (34) can be rewritten according to the above definition:

$$\ddot{\boldsymbol{e}} - \ddot{\boldsymbol{e}}_d + \boldsymbol{L}_v(\dot{\boldsymbol{e}} - \dot{\boldsymbol{e}}_d) + \boldsymbol{L}_p(\boldsymbol{e} - \boldsymbol{e}_d) = \boldsymbol{0}. \tag{43}$$

Substituting (6) into (31), we have

$$\boldsymbol{H}_d\ddot{\boldsymbol{x}}_d + \boldsymbol{C}_d\dot{\boldsymbol{x}}_d + \boldsymbol{K}_d\boldsymbol{x}_d - \boldsymbol{K}_d'\boldsymbol{x}_0 + \boldsymbol{H}_m\ddot{\boldsymbol{x}} + \boldsymbol{C}_m\dot{\boldsymbol{x}} + \boldsymbol{G}_m\boldsymbol{x} = \boldsymbol{0}. \tag{44}$$

Comparing (38) with (44), we can obtain

$$\boldsymbol{H}_d\ddot{\boldsymbol{e}}_d + \boldsymbol{C}_d\dot{\boldsymbol{e}}_d + \boldsymbol{K}_d\boldsymbol{e}_d + \boldsymbol{H}_m\ddot{\boldsymbol{e}} + \boldsymbol{C}_m\dot{\boldsymbol{e}} + \boldsymbol{G}_m\boldsymbol{e} = \boldsymbol{0}. \tag{45}$$

Comparing (43) with (45), we have

$$\begin{aligned}\ddot{\boldsymbol{e}} = &- \boldsymbol{H}_t^{-1}(\boldsymbol{H}_d\boldsymbol{L}_v + \boldsymbol{C}_m)\,\dot{\boldsymbol{e}} - \boldsymbol{H}_t^{-1}\left(\boldsymbol{H}_d\boldsymbol{L}_p + \boldsymbol{G}_m\right)\boldsymbol{e} \\ &+ \boldsymbol{H}_t^{-1}(\boldsymbol{H}_d\boldsymbol{L}_v - \boldsymbol{C}_d)\,\dot{\boldsymbol{e}}_d + \boldsymbol{H}_t^{-1}\left(\boldsymbol{H}_d\boldsymbol{L}_p - \boldsymbol{K}_d\right)\boldsymbol{e}_d\end{aligned} \tag{46}$$

and

$$\begin{aligned}\ddot{\boldsymbol{e}}_d = &- \boldsymbol{H}_t^{-1}(\boldsymbol{H}_m\boldsymbol{L}_v + \boldsymbol{C}_d)\dot{\boldsymbol{e}}_d - \boldsymbol{H}_t^{-1}(\boldsymbol{H}_m\boldsymbol{L}_p + \boldsymbol{K}_d)\boldsymbol{e}_d \\ &+ \boldsymbol{H}_t^{-1}(\boldsymbol{H}_m\boldsymbol{L}_v - \boldsymbol{C}_m)\dot{\boldsymbol{e}} + \boldsymbol{H}_t^{-1}(\boldsymbol{H}_m\boldsymbol{L}_p - \boldsymbol{G}_m)\boldsymbol{e}.\end{aligned} \tag{47}$$

The switched system can be described as:

$$\dot{\boldsymbol{E}} = \begin{cases}\boldsymbol{A}_i\boldsymbol{E}, & t_u + c\delta \le t \le t_u + (c + 1 - \alpha)\delta \\ \boldsymbol{A}_a\boldsymbol{E}, & t_u + (c + 1 - \alpha)\delta < t < t_u + (c + 1)\delta\end{cases} \tag{48}$$

where $\boldsymbol{E} = [\boldsymbol{e}^T, \dot{\boldsymbol{e}}^T, \boldsymbol{e}_d^T, \dot{\boldsymbol{e}}_d^T]^T$. From (40) and (42), we have

$$\boldsymbol{A}_i = \begin{bmatrix}\boldsymbol{A}_{i1} & \boldsymbol{0} \\ \boldsymbol{A}_{i1} - \boldsymbol{A}_{i2} & \boldsymbol{A}_{i2}\end{bmatrix} \tag{49}$$

where

$$\boldsymbol{A}_{i1} = \begin{bmatrix}\boldsymbol{0} & \boldsymbol{I}_n \\ -\boldsymbol{H}_t^{-1}(\boldsymbol{K}_d + \boldsymbol{G}_m) & -\boldsymbol{H}_t^{-1}(\boldsymbol{C}_d + \boldsymbol{C}_m)\end{bmatrix},$$

$$\boldsymbol{A}_{i2} = \begin{bmatrix}\boldsymbol{0} & \boldsymbol{I}_n \\ -\boldsymbol{L}_p & -\boldsymbol{L}_v\end{bmatrix}.$$

From (46) and (47), we have

$$\boldsymbol{A}_a = \begin{bmatrix}\boldsymbol{A}_{a1} & \boldsymbol{A}_{a2} \\ \boldsymbol{A}_{a3} & \boldsymbol{A}_{a1} + \boldsymbol{A}_{a2} - \boldsymbol{A}_{a3}\end{bmatrix} \tag{50}$$

https://doi.org/10.1017/S0263574723001601 Published online by Cambridge University Press

where

$$\boldsymbol{A}_{a1} = \begin{bmatrix} \mathbf{0} & \boldsymbol{I}_n \\ -\boldsymbol{H}_t^{-1}(\boldsymbol{H}_d\boldsymbol{L}_p + \boldsymbol{G}_m) & -\boldsymbol{H}_t^{-1}(\boldsymbol{H}_d\boldsymbol{L}_v + \boldsymbol{C}_m) \end{bmatrix},$$

$$\boldsymbol{A}_{a2} = \begin{bmatrix} \mathbf{0} & \mathbf{0} \\ \boldsymbol{H}_t^{-1}\left(\boldsymbol{H}_d\boldsymbol{L}_p - \boldsymbol{K}_d\right) & \boldsymbol{H}_t^{-1}(\boldsymbol{H}_d\boldsymbol{L}_v - \boldsymbol{C}_d) \end{bmatrix},$$

$$\boldsymbol{A}_{a3} = \begin{bmatrix} \mathbf{0} & \mathbf{0} \\ \boldsymbol{H}_t^{-1}(\boldsymbol{H}_m\boldsymbol{L}_p - \boldsymbol{G}_m) & \boldsymbol{H}_t^{-1}(\boldsymbol{H}_m\boldsymbol{L}_v - \boldsymbol{C}_m) \end{bmatrix}.$$

Remark 3. Compared with [29], the proposed hybrid system framework is suitable for the second-order environment, and the states of the two subsystems of the switched system are of the same dimension and keep continuous during the control process without the state mappings and periodic resetting operation. Therefore, more general analysis methods of switched systems can be applied, which enables more advanced impedance or admittance controllers to be added to the proposed framework, showing its wider scope of application.

Remark 4. Impedance control required by the proposed impedance adaptation method can be easily realized by setting $\alpha = 0$ in the proposed hybrid system framework, which shows the flexibility of the proposed control scheme.

3.4. Stability analysis

To prove the stability of the switched system, the definition of discrete equivalent (DE) proposed by Das and Mukherjee [34] is given first. The time-invariant linear system

$$\dot{\boldsymbol{E}} = \boldsymbol{A}_{eq}\boldsymbol{E} \tag{51}$$

is a DE of a switched linear system if the states of both systems are assumed to take the same values at regular time intervals and evolve from the same initial condition.

Then, we analyze the switched system (48) calculated from the nominal robot–environment interaction dynamics, and the relation between the states of the switched system at time $t = t_u + c\delta$ and $t = t_u + (c+1)\delta$ can be obtained from (48), $c = 0, 1, 2, \cdots$:

$$\begin{aligned} \boldsymbol{E}(t_u + (c+1-\alpha)\delta) &= e^{\boldsymbol{A}_i(1-\alpha)\delta}\boldsymbol{E}(t_u + c\delta) \\ \Rightarrow \boldsymbol{E}(t_u + (c+1)\delta) &= e^{\boldsymbol{A}_a\alpha\delta}\boldsymbol{E}(t_u + (c+1-\alpha)\delta) \\ &= e^{\boldsymbol{A}_a\alpha\delta}e^{\boldsymbol{A}_i(1-\alpha)\delta}\boldsymbol{E}(t_u + c\delta). \end{aligned} \tag{52}$$

According to (51) and (52), the system (51) becomes a DE of the switched system (48) with

$$\boldsymbol{A}_{eq} = \frac{1}{\delta}\ln\left[e^{\boldsymbol{A}_a\alpha\delta}e^{\boldsymbol{A}_i(1-\alpha)\delta}\right] \tag{53}$$

where $\boldsymbol{A}_{eq}$ is the logarithm of a matrix with a specific form, whose existence and uniqueness problems are fully discussed in ref. [34]. It can be observed that if the states of the corresponding DE system (51) converge to the equilibrium point and the states of the switched system (48) are bounded within all time intervals, then the stability of the switched system at the same equilibrium point can be proven. To proceed, a more straightforward proof of the stability condition of the switched system than ref. [29] is given as follows:

Theorem 3.1. *Exponential Stability: The switched system* (48) *is exponentially stable at the equilibrium point* $\boldsymbol{E} = \mathbf{0}$ *if* $\boldsymbol{A}_{eq}$ *of the DE system* (51) *is Hurwitz.*

https://doi.org/10.1017/S0263574723001601 Published online by Cambridge University Press

Proof. First, we assume the norm of the initial state of the DE system satisfies $\|\boldsymbol{E}(t_u)\| = \beta$. Using the Hurwitz property of $\boldsymbol{A_{eq}}$ and the DE system (51), we have

$$\begin{aligned}\boldsymbol{E}(t) &= e^{\boldsymbol{A_{eq}}(t-t_u)}\boldsymbol{E}(t_u)\\ \Rightarrow \|\boldsymbol{E}(t)\| &\le \|e^{\boldsymbol{A_{eq}}(t-t_u)}\|\|\boldsymbol{E}(t_u)\|\\ &\le \gamma e^{-\sigma(t-t_u)}\beta\end{aligned} \tag{54}$$

where $\gamma, \sigma > 0$. Since the states of the switched system and its DE are assumed to take the same values at time $t = t_u + c\delta$, $c = 0, 1, 2, \cdots$, the states of the switched system (48) satisfy

$$\|\boldsymbol{E}(t_u + c\delta)\| \le \gamma\beta e^{-\sigma c\delta}. \tag{55}$$

Consider the time interval $t_u + c\delta \le t \le t_b + (c+1)\delta$, in which the subinterval $t_u + c\delta \le t \le t_b + c\delta + (1-\alpha)\delta$ for impedance control is considered first. Using (55) and the relation $t = t_u + c\delta + \lambda_i$, $0 \le \lambda_i \le (1-\alpha)\delta$, we have

$$\begin{aligned}\boldsymbol{E}(t_u + c\delta + \lambda_i) &= e^{\boldsymbol{A_i}\lambda_i}\boldsymbol{E}(t_u + c\delta)\\ \Rightarrow \|\boldsymbol{E}(t_u + c\delta + \lambda_i)\| &\le \|e^{\boldsymbol{A_i}\lambda_i}\|\|\boldsymbol{E}(t_u + c\delta)\|\\ &\le e^{\eta_i\lambda_i}\gamma\beta e^{-\sigma c\delta}\\ \Rightarrow \|\boldsymbol{E}(t)\| &\le e^{\eta_i\lambda_i}\gamma\beta e^{-\sigma(t-t_u-\lambda_i)}\\ &\le \gamma\beta e^{(\eta_i+\sigma)(1-\alpha)\delta}e^{-\sigma(t-t_u)}\end{aligned} \tag{56}$$

where $\eta_i = \|\boldsymbol{A_i}\|$. From (56), we can obtain

$$\|\boldsymbol{E}(t_u + c\delta + (1-\alpha)\delta)\| \le \gamma\beta e^{\eta_i(1-\alpha)\delta}e^{-\sigma c\delta}. \tag{57}$$

Then consider the subinterval $t_u + c\delta + (1-\alpha)\delta \le t \le t_b + (c+1)\delta$ for admittance control. Using (57) and the relation $t = t_u + c\delta + (1-\alpha)\delta + \lambda_a$, $0 \le \lambda_a \le \alpha\delta$, we have

$$\begin{aligned}&\boldsymbol{E}(t_u + c\delta + (1-\alpha)\delta + \lambda_a)\\ &\quad= e^{\boldsymbol{A_a}\lambda_a}\boldsymbol{E}(t_u + c\delta + (1-\alpha)\delta)\\ \Rightarrow &\|\boldsymbol{E}(t_u + c\delta + (1-\alpha)\delta + \lambda_a)\|\\ &\quad\le \|e^{\boldsymbol{A_a}\lambda_a}\|\|\boldsymbol{E}(t_u + c\delta + (1-\alpha)\delta)\|\\ &\quad\le e^{\eta_a\lambda_a}\gamma\beta e^{\eta_i(1-\alpha)\delta}e^{-\sigma c\delta}\\ \Rightarrow &\|\boldsymbol{E}(t)\| \le e^{\eta_a\lambda_a}\gamma\beta e^{\eta_i(1-\alpha)\delta}e^{-\sigma(t-t_u-(1-\alpha)\delta-\lambda_a)}\\ &\quad\le \gamma\beta e^{(\eta_i+\sigma)(1-\alpha)\delta}e^{(\eta_a+\sigma)\alpha\delta}e^{-\sigma(t-t_u)}\end{aligned} \tag{58}$$

where $\eta_a = \|\boldsymbol{A_a}\|$. From (56) and (58), in the time interval $t_u + c\delta \le t \le t_b + (c+1)\delta$, $c = 0, 1, 2, \cdots$, the states of the switched system satisfy

$$\begin{aligned}\|\boldsymbol{E}(t)\| &\le \gamma\beta\rho e^{-\sigma(t-t_u)},\\ \rho &= \max[e^{(\eta_i+\sigma)(1-\alpha)\delta}, e^{(\eta_i+\sigma)(1-\alpha)\delta}e^{(\eta_a+\sigma)\alpha\delta}]\\ &= e^{(\eta_i+\sigma)(1-\alpha)\delta}e^{(\eta_a+\sigma)\alpha\delta}\end{aligned} \tag{59}$$

which proves the exponential stability of $\boldsymbol{E} = \boldsymbol{0}$ for the switched system. □

https://doi.org/10.1017/S0263574723001601 Published online by Cambridge University Press

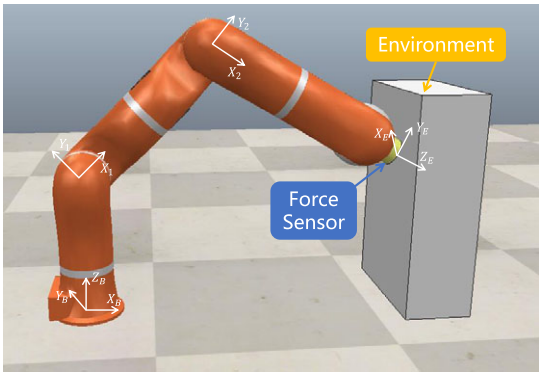

Figure 7. *Simulation scenario: the manipulator interacts with the second-order unknown environment in the X-direction.*

3.5. Mapping of the optimal duty cycle

To provide the optimal implementation performance for the obtained target impedance model, the optimal intermediate controller corresponding to the optimal duty cycle α^* needs to be selected to minimize the cost function [32]:

$$J_2 = \frac{1}{2}\int_{t_u}^{t_f} \boldsymbol{e}^T \boldsymbol{e} dt = \frac{1}{2}\int_{t_u}^{t_f} (\boldsymbol{x} - \boldsymbol{x}_{\boldsymbol{ref}})^T (\boldsymbol{x} - \boldsymbol{x}_{\boldsymbol{ref}}) dt \tag{60}$$

where t_u and t_f are the initial and end time of control, respectively. However, an explicit expression of the optimal duty cycle is difficult to obtain, since the duty cycle does not explicitly appear in the state equation of the switched system but affects the system by changing the switching time. Moreover, not only the different environments but also the different target impedance models make an impact on the performance of the switching controller. Therefore, we utilize the strong relation between the environmental stiffness and the optimal duty cycle and we only consider one dimension for analysis without the loss of generality. For the system (20) and the cost function (24), we define the optimal feedback gain and the corresponding desired stiffness obtained by LQR as $k^* = [k_1^*, k_2^*, k_3^*]$ and $k_d^* = -k_2^*$, respectively, which is similar to (25). Substituting (12) and (22) into (11), we can extract the environmental stiffness k_e from the desired stiffness k_d^* directly:

$$k_e = -\frac{1}{2}\left(k_d^* - \frac{Q_2}{Rk_d^*}\right) \tag{61}$$

where the weights Q_2 and R become scalars in one dimension. Hence, the mapping of the desired stiffness k_d^* to the optimal duty cycle α^* can be achieved. Given a desired stiffness k_d^*, the optimal target impedance model can be solved by LQR according to the environmental stiffness k_e from (61), so the values of the above cost function are calculated for the duty cycle $\alpha \in [0, 1]$ and the optimal duty cycle which minimizes the cost function can be found.

4. Simulation studies

To verify the interaction and optimal impedance implementation capabilities of the proposed HIAC scheme, simulations are performed on a 2-DOF manipulator in this section. For the simulation setup, the manipulator is considered to interact with the second-order unknown environment, and the external force is applied along the X-direction and can be measured by a force sensor mounted on the end effector, as shown in Fig. 7. In practice, the actual robot dynamics including uncompensated joint friction,

https://doi.org/10.1017/S0263574723001601 Published online by Cambridge University Press

Table I. *Parameters of the simulated manipulator.*

Parameters	Description	Value
m_1	Mass of link 1	1.0 kg
m_2	Mass of link 2	1.0 kg
$\hat{m}_1$	Estimated mass of link 1	0.95 kg
$\hat{m}_2$	Estimated mass of link 2	0.95 kg
l_1	Length of link 1	0.8 m
l_2	Length of link 2	0.8 m
c_v	Coefficient of viscous friction	0.4 Nms/rad
τ_c	Coefficient of Coulomb friction	0.1 Nm

model uncertainties, time delays, and noises in the external force measurement are considered in the simulation:

$$\hat{\boldsymbol{H}}(\boldsymbol{q})\ddot{\boldsymbol{q}} + \hat{\boldsymbol{C}}(\boldsymbol{q}, \dot{\boldsymbol{q}})\dot{\boldsymbol{q}} + \hat{\boldsymbol{G}}(\boldsymbol{q}) = \boldsymbol{\tau}_c + \boldsymbol{\tau}_f + \hat{\boldsymbol{J}}^T(\boldsymbol{q})\hat{\boldsymbol{F}}_e \tag{62}$$

where $\hat{\boldsymbol{H}}(\boldsymbol{q})$, $\hat{\boldsymbol{C}}(\boldsymbol{q}, \dot{\boldsymbol{q}})$, and $\hat{\boldsymbol{G}}(\boldsymbol{q})$ are the estimated inertia matrix, estimated Coriolis and Centrifugal force matrix, and estimated gravitational force vector in joint space, respectively. $\hat{\boldsymbol{J}}$, $\hat{\boldsymbol{F}}_e$, and $\boldsymbol{\tau}_f$ are the estimated Jacobian matrix, estimated interaction force, and uncompensated joint friction, respectively. Then, the above kinematic and dynamics parameters are given as:

$$\begin{aligned}
\hat{\boldsymbol{H}}(\boldsymbol{q}) &= \begin{bmatrix} \hat{m}_2 l_2^2 + 2\hat{m}_2 l_1 l_2 c_2 + (\hat{m}_1 + \hat{m}_2) l_1^2 & \hat{m}_2 l_2^2 + \hat{m}_2 l_1 l_2 c_2 \\ \hat{m}_2 l_2^2 + \hat{m}_2 l_1 l_2 c_2 & \hat{m}_2 l_2^2 \end{bmatrix} \\
\hat{\boldsymbol{C}}(\boldsymbol{q}, \dot{\boldsymbol{q}}) &= \begin{bmatrix} -\hat{m}_2 l_1 l_2 s_2 \dot{q}_2 & -\hat{m}_2 l_1 l_2 s_2 (\dot{q}_1 + \dot{q}_2) \\ \hat{m}_2 l_1 l_2 s_2 \dot{q}_1 & 0 \end{bmatrix}, \hat{\boldsymbol{G}}(\boldsymbol{q}) = \begin{bmatrix} \hat{m}_2 l_2 g c_{12} + (\hat{m}_1 + \hat{m}_2) l_1 g c_1 \\ \hat{m}_2 l_2 g c_{12} \end{bmatrix} \\
\hat{\boldsymbol{J}} &= \begin{bmatrix} -(l_1 s_1 + l_2 s_{12}) + g_n & -l_2 s_{12} + g_n \\ l_1 c_1 + l_2 c_{12} + g_n & l_2 c_{12} + g_n \end{bmatrix}, \boldsymbol{\tau}_f = -\begin{bmatrix} c_v \dot{q}_1 + \text{sign}(\dot{q}_1)\tau_c \\ c_v \dot{q}_2 + \text{sign}(\dot{q}_2)\tau_c \end{bmatrix} \\
\hat{\boldsymbol{F}}_e(t) &= \boldsymbol{F}_e(t - 6t_s) + [g_n, g_n]^T
\end{aligned} \tag{63}$$

where the sampling time of the simulations is set as $t_s = 1$ ms and $g_n \sim \mathcal{N}(0, 0.01)$ is the Gaussian noise. Table I presents the parameters of the simulated manipulator. The parameters of the second-order environments are described by:

$$\boldsymbol{H}_m = \begin{bmatrix} 0.1 & 0 \\ 0 & 0 \end{bmatrix}, \boldsymbol{C}_m = \begin{bmatrix} 1 & 0 \\ 0 & 0 \end{bmatrix}, \boldsymbol{G}_m = \begin{bmatrix} k_e & 0 \\ 0 & 0 \end{bmatrix} \tag{64}$$

where k_e is the environmental stiffness in the X-direction. The soft, medium, and stiff environments corresponding to the environments with low stiffness $k_e = 20$ N/m, medium stiffness $k_e = 150$ N/m, and high stiffness $k_e = 1000$ N/m, respectively, are considered and assumed to have the same inertia and damping. Note that the environmental parameters are unknown in the simulation.

4.1. Interaction capability

In this part, the effectiveness of the proposed impedance adaptation method is verified and the parameters are considered only in the X-direction. The parameters in (21) are set as $U = -0.5$ and $V = 0.3$. The weights in (24) are set as $Q_1 = 1$, $Q_2 = 30,000$, and $R = 1$ to cope with the environments (64) which cover a wide range of stiffness. The initial feedback gain is chosen as $\boldsymbol{K_0} = [-1, -1500, 1500]^T$, and the initial $\boldsymbol{Y_k}$ is set as $\boldsymbol{Y_0} = 10\boldsymbol{I_m}$. The exploration noise is designed as $\nu = -\sum_{\omega=1}^{4} (180/\omega)\sin(\omega t)$. The preset threshold is set as $\varepsilon = 0.001$, and the transitional time is set as $T_s = 2$s.

https://doi.org/10.1017/S0263574723001601 Published online by Cambridge University Press

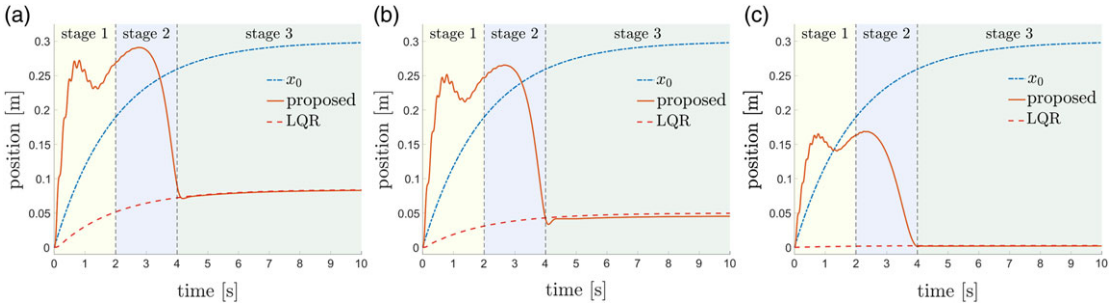

Figure 8. *Virtual equilibrium and actual trajectories in the (a) soft, (b) medium, and (c) stiff environments. For the proposed method, in stage 1 (yellow region), the system input is set as* $\boldsymbol{u} = -\boldsymbol{K_0}\boldsymbol{\xi} + \boldsymbol{v}$ *and the system information is collected until the rank condition (14) is satisfied. In stage 2 (blue region), the optimal feedback gain* $\boldsymbol{K_k}$ *is solved, and the system input is set as* $\boldsymbol{u} = -\boldsymbol{K_k'}\boldsymbol{\xi} + \boldsymbol{v'}$ *to keep the system input continuous until* $t > t_l + T_s$. *In stage 3 (green region), the system input becomes* $\boldsymbol{u} = -\boldsymbol{K_k}\boldsymbol{\xi}$.

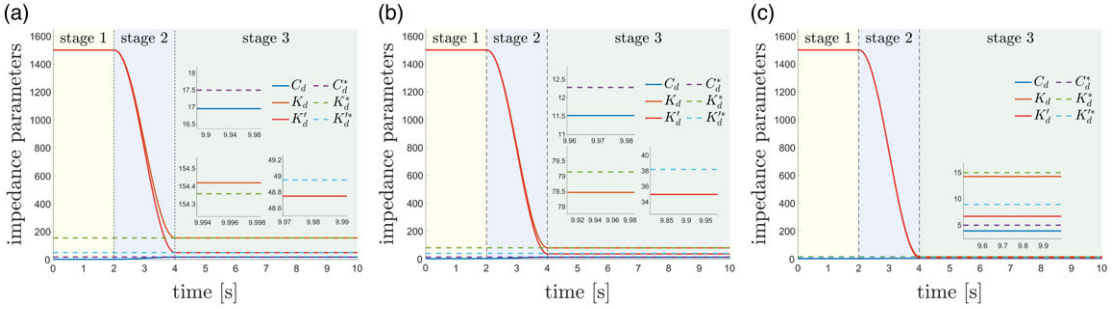

Figure 9. *Impedance parameters in the (a) soft, (b) medium, and (c) stiff environments.* $\boldsymbol{C_d}$, $\boldsymbol{K_d}$, *and* $\boldsymbol{K_d'}$ *are adapted by the proposed method.* $\boldsymbol{C_d^*}$, $\boldsymbol{K_d^*}$, *and* $\boldsymbol{K_d'^*}$ *are solved by LQR.*

The simulation results are presented in Figs. 8 and 9. LQR is regarded as the comparison method which can solve ARE using the known matrices $\boldsymbol{A}$ and $\boldsymbol{B}$ to obtain the optimal target impedance model, while the proposed method is suitable for the case where the environment dynamics are unknown, that is, the matrices $\boldsymbol{A}$ and $\boldsymbol{B}$ are unknown. The virtual equilibrium trajectories and actual trajectories of LQR and the proposed method in the soft, medium, and stiff environments are shown in Fig. 8. In any case, an obvious error exists in the actual trajectories between LQR and the proposed method in phase 1 (yellow region) due to the obvious difference between the target impedance model $F_e = \ddot{x} + \dot{x} + 1500(x - x_0) + \nu$ equivalent to the initial system input and the optimal target impedance model obtained by LQR. In addition, the exploration noise results in trajectory jitters of the proposed method, which is inevitable because rich state and input information is required to ensure that the system meets the PE condition so that the rank condition (14) is satisfied. In phase 2 (blue region), the transitional system input works so that the trajectory error rises slightly for a short time and then decreases smoothly. In phase 3 (green region), the actual trajectory of the proposed method converges to a small neighborhood of the actual trajectory of LQR.

The impedance parameters of LQR and the proposed method in the soft, medium, and stiff environments are shown in Fig. 9. The impedance parameters adapted by the proposed method change smoothly during stage 2 and converges to a small neighborhood of the impedance parameters of LQR in stage 3. Table II presents the target impedance models obtained by LQR and the proposed method in the soft, medium, and stiff environments. It can be seen that the models obtained by the proposed method are second-order and are quite close to the corresponding optimal models obtained by LQR

https://doi.org/10.1017/S0263574723001601 Published online by Cambridge University Press

Table II. *Simulated target impedance models.*

Environments	LQR	Proposed method
Soft	$F_e = \ddot{x} + 17.48\dot{x} + 154.36x - 48.95x_0$	$F_e = \ddot{x} + 16.93\dot{x} + 154.43x - 48.74x_0$
Medium	$F_e = \ddot{x} + 12.27\dot{x} + 79.13x - 38.13x_0$	$F_e = \ddot{x} + 11.50\dot{x} + 78.46x - 34.91x_0$
Stiff	$F_e = \ddot{x} + 4.90\dot{x} + 14.89x - 8.84x_0$	$F_e = \ddot{x} + 3.82\dot{x} + 14.16x - 6.59x_0$

in the second-order environments, which proves the ability of the proposed method to obtain the target impedance model representing the optimal interaction behavior without the accurate environment dynamics. Moreover, it is noteworthy that as the environmental stiffness increases, the desired stiffness and damping of the target impedance model obtained by the proposed method decrease. In other words, as the environment becomes stiffer, the desired interaction behavior obtained by the proposed method becomes softer, which shows good adaptability of the proposed method to different environments.

4.2. Impedance implementation capability

In this part, a fixed target impedance model is implemented in the environments (64) to illustrate the effectiveness of the proposed hybrid system framework. Specifically, the switching control law (35) is implemented using (28) and (32), and the desired trajectory $\boldsymbol{x_d}$ is updated using (37) and (31) during impedance and admittance control phases, respectively. Note that the ideal trajectory $\boldsymbol{x_{ref}}$ is not used in the control process. The parameters of the fixed target impedance model to be implemented are chosen as $\boldsymbol{H_d} = 1.0\boldsymbol{I_2}$, $\boldsymbol{C_d} = 4\boldsymbol{I_2}$, $\boldsymbol{K_d} = 10\boldsymbol{I_2}$, and $\boldsymbol{K_d'} = 5\boldsymbol{I_2}$. The switching period is designed as $\delta = 0.02$ s, and the control gains of the inner loop controller of admittance control are designed with high gain as $\boldsymbol{L_p} = 10^6\boldsymbol{I_2}$ and $\boldsymbol{L_v} = 500\boldsymbol{I_2}$ to be robust to the system uncertainties and make $\boldsymbol{A_{eq}}$ Hurwitz. The virtual equilibrium trajectory in the X-direction is designed as $x_0 = 1 + \sin(8t)$ m.

The ideal trajectories $\boldsymbol{x_{ref}}$ for the fixed target impedance model in different environments are calculated by (38) and shown in Fig. 10(a). The trajectory errors of different controllers for the fixed target impedance model in the soft, medium, and stiff environments are shown in Fig. 10(b)–(d), respectively, where impedance, admittance, and the intermediate controllers with different duty cycle parameters are introduced. In the soft environment, impedance control results in relatively large tracking error and steady-state error due to the uncompensated friction, while admittance control has better performance, which is shown as high position accuracy. As the environmental stiffness increases, the performance of impedance control improves, shown as the decrease in steady-state error, while the performance of admittance control deteriorates, shown as the increase in oscillations, due to the time delay of the external force measurement and the high gains of the inner loop controller. Finally, for the stiff environment, admittance control leads to large oscillations, while impedance control imparts good robustness to the system, which is shown as small oscillations and negligible steady-state error.

Moreover, it can be seen from Fig. 10 that the response of the intermediate controller corresponding to a smaller duty cycle is closer to the response of impedance control, and as the duty cycle increases, it tends to the response of admittance control. Therefore, the proposed framework can generate interpolation between the responses of impedance control and admittance control by properly selecting the duty cycle, showing its applicability to the second-order environments and its potential to provide good control performance independent of the environmental stiffness, which is illustrated in the following section.

4.3. Optimal implementation capability

In this part, the proposed hybrid system framework's capability to provide the optimal implementation performance for the target impedance models using the mapping of the optimal duty cycle is evaluated. The initial time and end time of control are set as $t_u = 0$ s and $t_f = 2$ s, respectively. The target impedance models to be implemented are obtained by the proposed impedance adaptation method and shown in

https://doi.org/10.1017/S0263574723001601 Published online by Cambridge University Press

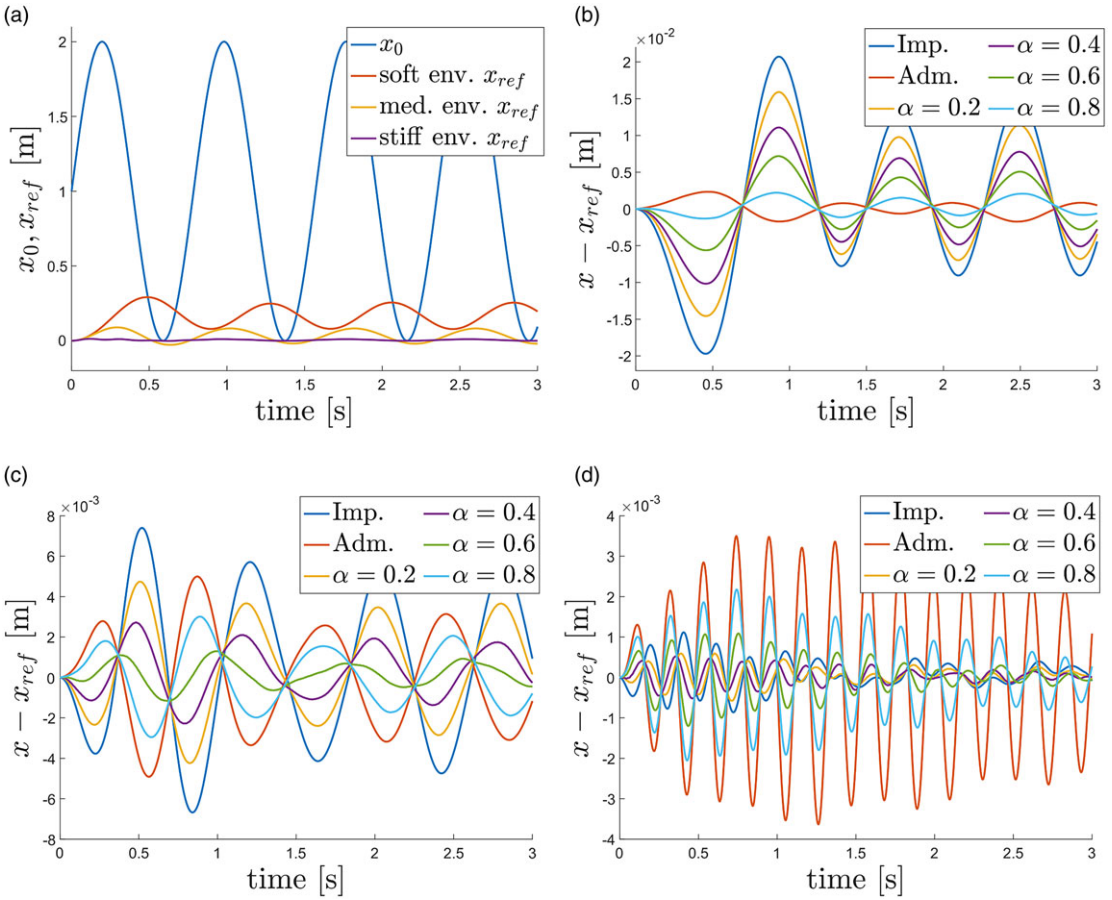

Figure 10. *(a) Virtual equilibrium and ideal trajectories. Trajectory errors of different controllers for the fixed target impedance model in the (b) soft, (c) medium, and (d) stiff environments.*

Table II. The remaining parameters are the same as above. Considering the desired stiffness k_d^* in range [10, 170], the mapping is built offline and shown in Fig. 11(a), where we can see that the optimal duty cycle becomes larger as the desired behavior becomes stiffer, and the optimal duty cycle has a minimum interval of $t_s/\delta = 0.05$ between [0, 1]. The optimal duty cycles corresponding to the desired stiffness in the soft, medium, and stiff environments can be obtained as $\alpha^* = 0.85$, $\alpha^* = 0.55$, and $\alpha^* = 0.3$ from the mapping, respectively. It should be noted that the estimated environmental stiffness is implicitly used as an intermediate variable during this process as shown in (61), and the target impedance models remain constant after impedance adaptation.

Figure 11(b) shows the virtual equilibrium and ideal trajectories for the corresponding target impedance models in different environments. The trajectory errors of different controllers for the corresponding target impedance model in the soft, medium, and stiff environments are shown in Fig. 11(c)–(e), where impedance, admittance, and the intermediate controllers corresponding to different duty cycles are introduced. In Fig. 11(c)–(e), impedance control and admittance control show similar characteristics to those in the previous section for the same environment. In the soft environment, the response of the optimal intermediate controller is close to the response of admittance control, and a higher position accuracy than that of admittance control is obtained. In the medium environment, the response of the optimal intermediate controller tends to be the average of the responses of impedance and admittance controls, resulting in better tracking performance than both controllers. In the stiff environment, the response of the optimal intermediate controller tends to the response of impedance control,

https://doi.org/10.1017/S0263574723001601 Published online by Cambridge University Press

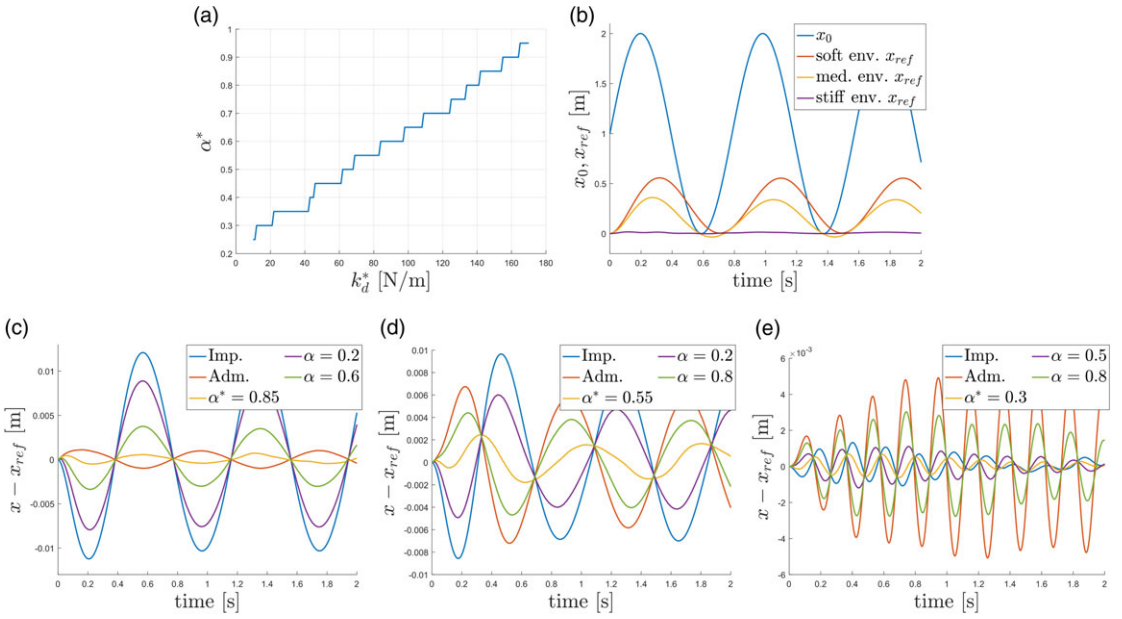

Figure 11. *(a) Mapping of the optimal duty cycle in the simulation. (b) Virtual equilibrium and ideal trajectories. The trajectory errors of different controllers for the corresponding target impedance models in the (c) soft, (d) medium, and (e) stiff environments.*

showing its good robustness. In addition, compared with the other two intermediate controllers, the optimal intermediate controller shows better tracking performance in different environments.

5. Experimental studies

In this section, the performance of the robot–environment interaction using the proposed HIAC scheme is demonstrated by experiments conducted on a 7-DOF Franka EMIKA panda robot, as shown in Fig. 12. For the experimental setup, the robot is connected to a workstation PC via Ethernet, and the Franka Control Interface (FCI) is used to achieve the real-time control loop running at 1 kHz. Meanwhile, the current status of the robot including the interaction force between the robot and the objects are obtained from FCI at 1 kHz. In the experiment, the robot will contact with the soft and stiff sponge objects along the z-axis using the proposed HIAC scheme and the comparison method. On the z-axis, the soft object's inertia, damping, and stiffness parameters are 0.1 kg, 2 Ns/m, and 500 N/m, respectively. The stiff object's inertia, damping, and stiffness parameters are 0.1 kg, 5 Ns/m, and 1500 N/m, respectively. First, the end-effector position of the robot is moved to [0.36, 0, 0.08] m, then it will contact with the objects by specifying the virtual equilibrium trajectory as:

$$\boldsymbol{x_0} = \left[0.36,\ 0,\ 0.08 - 0.05(1 - \exp(-t))\right]^T \tag{65}$$

To proceed, an experimental comparison between the proposed impedance adaptation method and the commonly used LQR method is conducted to obtain the optimal impedance parameters. In this part, the weights in (24) are set as $Q_1 = 1$, $Q_2 = 1000$, and $R = 0.001$. The initial feedback gain is chosen as $\boldsymbol{K_0} = [-100, -2500, 2500]^T$, and the initial $\boldsymbol{Y_k}$ is set as $\boldsymbol{Y_0} = \boldsymbol{I_m}$. The parameters in (21) are set as $U = -0.3$ and $V = 0.6$, and the exploration noise is designed as $v = -\sum_{\omega=1}^{8}(10/\omega)\sin(\omega t)$. For the proposed method, the impedance iteration will stop when $\|\boldsymbol{Y_k} - \boldsymbol{Y_{k-1}}\| \leq 0.001$ and the transition begins with the transitional time $T_s = 2$ s. However, for the LQR method, an accurate environment dynamics model is required to obtain the optimal impedance parameters through the Riccati equation [21].

https://doi.org/10.1017/S0263574723001601 Published online by Cambridge University Press

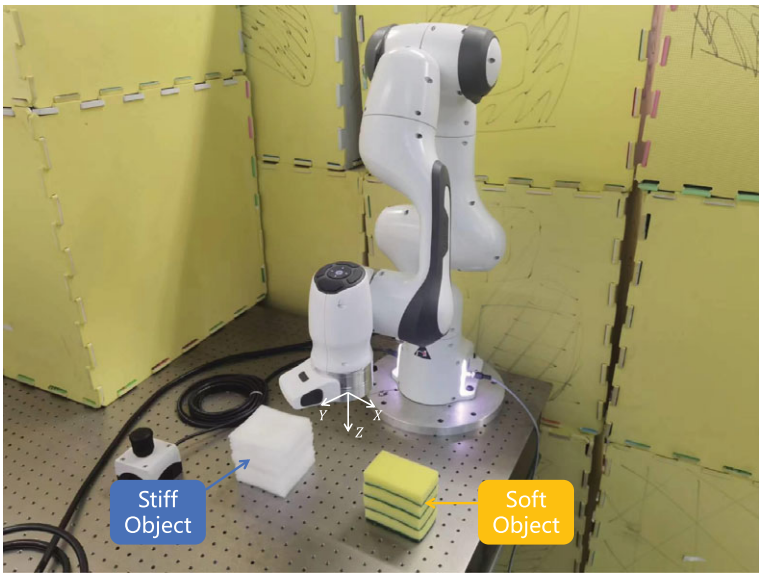

Figure 12. *Experimental scenario: Franka EMIKA panda robot interacts with the soft and stiff objects.*

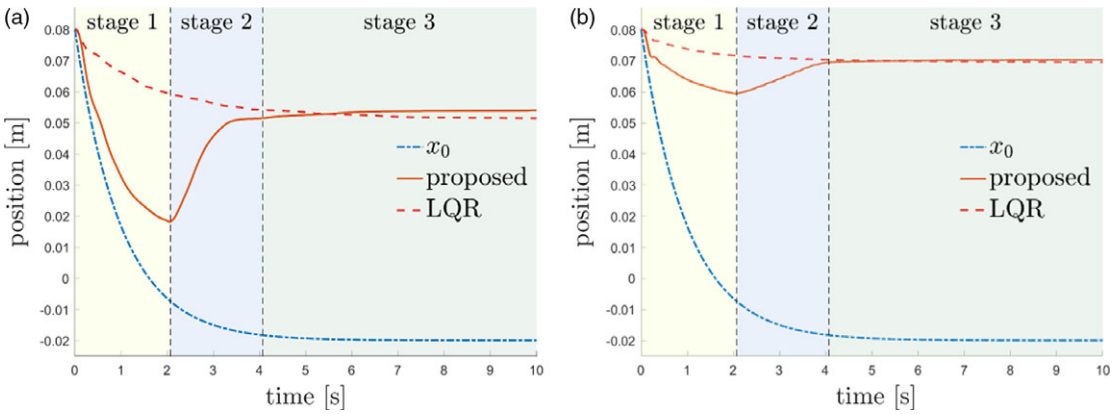

Figure 13. *Virtual equilibrium and actual experimental trajectories for the (a) soft and (b) stiff objects. The introduction of each stage is the same as Fig. 8.*

The experimental results are presented in Figs. 13–17. It can be seen that after impedance adaptation, the interaction behavior of the proposed method, including actual trajectory, interaction force, and impedance parameters, are close to those of the LQR method, which is consistent with the simulation results.

To further show the convergence performance of the impedance parameters obtained by the proposed method to the optimal values obtained by LQR more clearly, the errors of impedance parameters defined as $\|\boldsymbol{K}_k - \boldsymbol{K}^*\|$ are illustrated in Fig. 16, where the error decreases to around 5.92 after seven iterations for the soft object and decreases to around 6.45 after eight iterations for the stiff object. Table III presents the target impedance models obtained by LQR and the proposed method for the soft and stiff objects. It can be seen that the experimental error of damping parameters of the proposed method increases compared to simulation, which is mainly due to the influence of external noises on the velocity and force data collected in the experiment. In addition, Fig. 17 shows the control torques of seven robot joints during impedance adaptation for the soft and stiff objects. The maximum and average control torques for the

https://doi.org/10.1017/S0263574723001601 Published online by Cambridge University Press

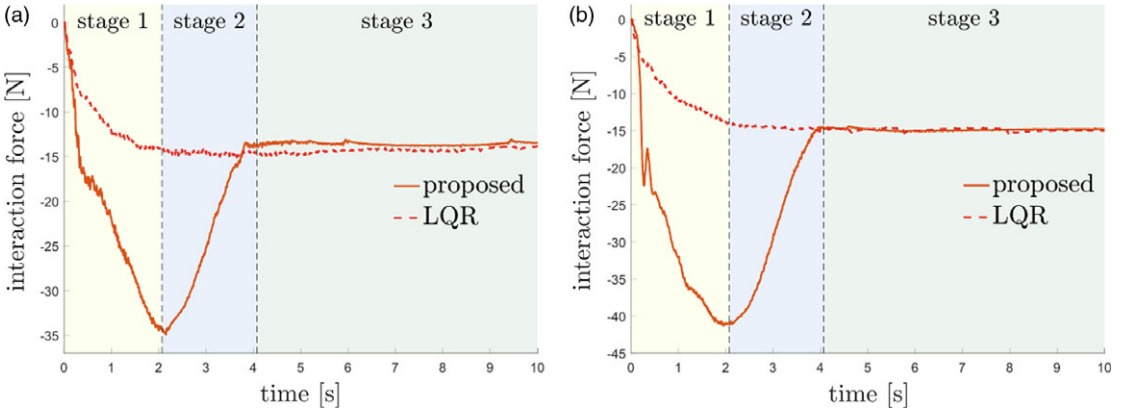

Figure 14. *Experimental interaction forces for the (a) soft and (b) stiff objects.*

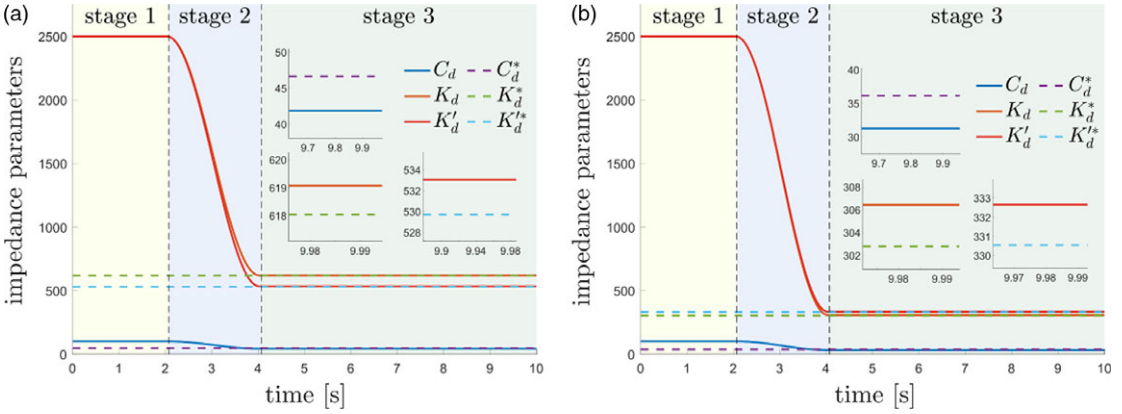

Figure 15. *Experimental impedance parameters for the (a) soft and (b) stiff objects.*

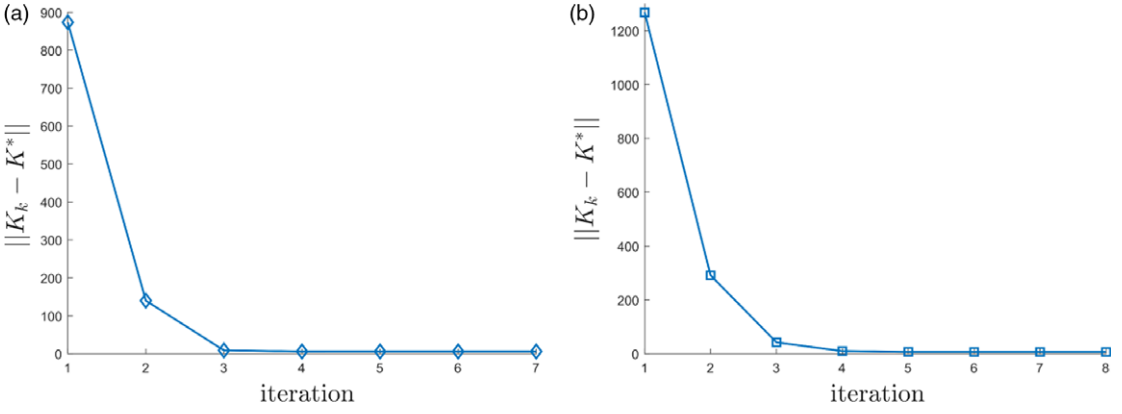

Figure 16. *Errors of experimental impedance parameters for the (a) soft and (b) stiff objects.*

interaction with the stiff object are larger than the soft object, and the second, fourth, and sixth joints bear the main output in the interaction.

Then, the proposed hybrid system framework is utilized to obtain the optimal implementation performance for the target impedance models using the mapping of the optimal duty cycle and compared with the hybrid controller in ref. [32]. For both the proposed and the comparison method, the initial time

https://doi.org/10.1017/S0263574723001601 Published online by Cambridge University Press

Table III. *Experimental target impedance models.*

Objects	LQR	Proposed method
Soft	$F_e = \ddot{x} + 46.62\dot{x} + 618.03x - 529.70x_0$	$F_e = \ddot{x} + 41.84\dot{x} + 619.06x - 533.04x_0$
Stiff	$F_e = \ddot{x} + 36.12\dot{x} + 302.78x - 330.54x_0$	$F_e = \ddot{x} + 31.23\dot{x} + 306.41x - 332.64x_0$

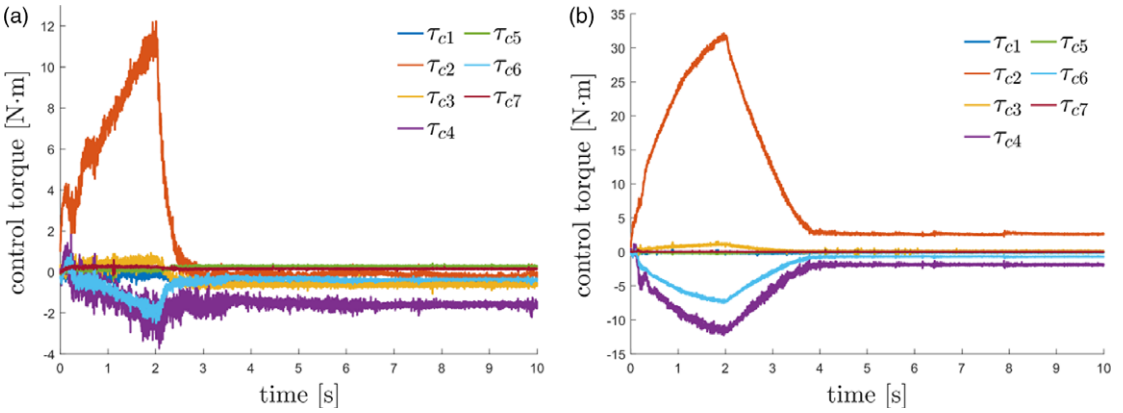

Figure 17. *Control torques of seven robot joints during impedance adaptation for the (a) soft and (b) stiff objects.*

and end time of control are set as $t_u = 0$ s and $t_f = 10$ s, respectively. The switching period is designed as $\delta = 0.02$ s, and the inner loop control gains of admittance control are designed as $L_p = 2000$ and $L_v = 1.4\sqrt{L_p}$ on the z-axis. The virtual equilibrium trajectory is the same as (65). Considering that the robot–environment interaction dynamics has been decoupled by the designed controller in each direction, the mapping of the optimal duty cycle on the z-axis for the proposed method in the experiment is generated through simulation using the above parameters, as shown in Fig. 18(a). According to the target impedance models in Table III, the optimal duty cycles of the proposed controller corresponding to the desired stiffness for the soft and stiff objects are obtained as $\alpha^* = 0.7$ and $\alpha^* = 0.5$ from the mapping, respectively. The optimal duty cycles of the hybrid controller in ref. [32] are assumed to be the same as those of the proposed controller.

To proceed, Fig. 18(b) shows the virtual equilibrium and ideal trajectories for the corresponding target impedance models. The trajectory errors of different controllers for the soft and stiff objects are illustrated in Fig. 18(c) and (d), where impedance, admittance, and the intermediate controllers corresponding to different duty cycles and the comparison controller in ref. [32] are introduced for the soft object, while admittance controller is not used for the stiff object because it will cause system instability. From Fig. 18(c) and (d), it can be seen that at the beginning, admittance controller for the soft object and the intermediate controller corresponding to $\alpha = 0.85$ for the stiff object cause relatively large oscillations due to their stiff characteristic and the uncertainties of the measured interaction force, while the optimal intermediate controllers have smoother performances and smaller transient tracking errors. Impedance controller results in large transient and steady-state tracking errors in the two cases due to its soft characteristic and unmodeled system dynamics, while the optimal intermediate controller has smaller steady-state errors. In addition, it can be observed that the comparison controller in ref. [32] initially results in a larger transient tracking error than the proposed controller because it only takes into account the spring environment and lacks feedforward velocity and acceleration terms in the admittance inner loop controller. From the above results, the proposed optimal intermediate controller chosen through the mapping exhibits better trajectory tracking performance than impedance, admittance, and the intermediate controllers corresponding to other duty cycles and the comparison controller in ref. [32] for the soft and stiff objects. Besides, Figs. 19 and 20 illustrate the control torques of seven robot joints

https://doi.org/10.1017/S0263574723001601 Published online by Cambridge University Press

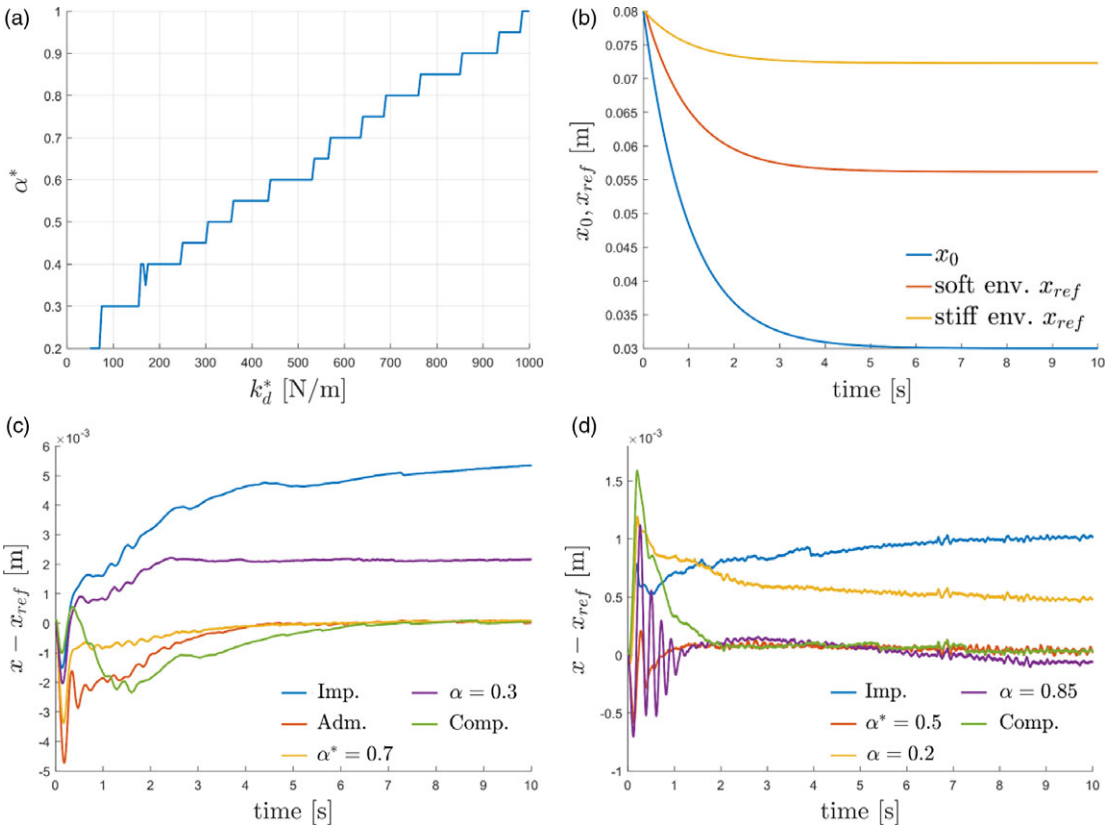

Figure 18. *(a) Mapping of the optimal duty cycle in the experiment. (b) Virtual equilibrium and ideal experimental trajectories. The trajectory errors of different controllers for the corresponding target impedance models for the (c) soft and (d) stiff objects.*

using different controllers for the corresponding target impedance models for the soft and stiff objects, respectively. It can be seen that the switching mechanism of the intermediate controller causes control torque vibration, which is difficult to completely avoid in practice, but can be limited to an acceptable range in the experiment by selecting appropriate parameters. Note that the control torque vibration of the comparison controller in ref. [32] is smaller than that of the proposed controller. One possible reason is that the admittance inner loop controller in ref. [32] is designed as a PD regulator, so the desired trajectory can be directly obtained during controller switching instead of its second derivative, thus avoiding integration error.

In summary, the proposed impedance adaptation method can obtain the optimal interaction behavior for the robot interacting with different second-order environments using the same control parameters without the accurate environment model; thus, it can be applied in more fields than LQR. The corresponding optimal intermediate controller is selected using the mapping of the optimal duty cycle, which enables the proposed hybrid system framework to combine the advantages of the good robustness of impedance control during stiff contact and the high position accuracy of admittance control during soft contact, thereby achieving better performance than impedance control or admittance control. For the cost function (60), the optimal implementation performance of the obtained target impedance models in different second-order environments is achieved. Therefore, the proposed HIAC scheme can solve the problem of obtaining and implementing optimal interaction behavior in complex unknown environments effectively.

https://doi.org/10.1017/S0263574723001601 Published online by Cambridge University Press

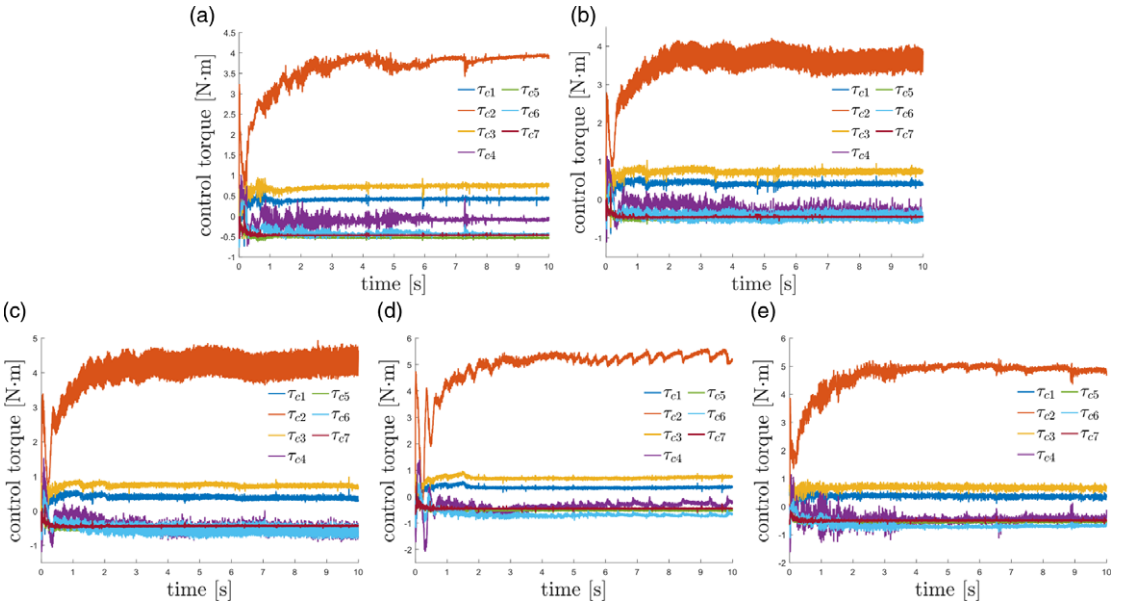

Figure 19. *Control torques of seven robot joints using different controllers for the corresponding target impedance models for the soft object. (a) Impedance controller, (b) intermediate controller corresponding to* $\alpha = 0.3$*, (c) optimal intermediate controller corresponding to* $\alpha^* = 0.7$*, (d) admittance controller, and (e) comparison controller.*

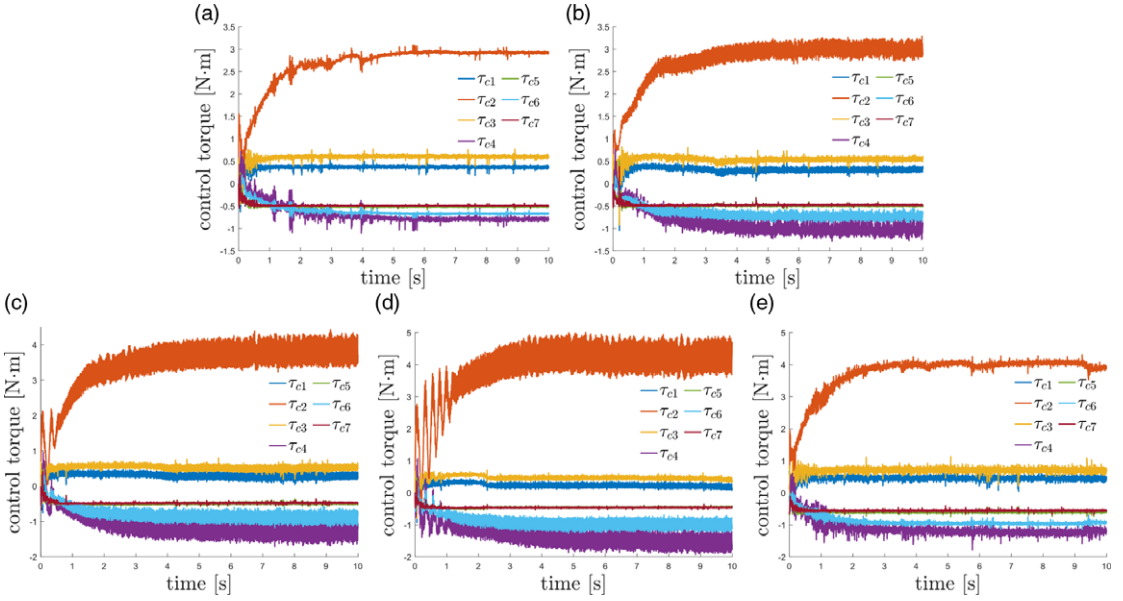

Figure 20. *Control torques of seven robot joints using different controllers for the corresponding target impedance models for the stiff object. (a) Impedance controller, (b) intermediate controller corresponding to* $\alpha = 0.2$*, (c) optimal intermediate controller corresponding to* $\alpha^* = 0.5$*, (d) intermediate controller corresponding to* $\alpha = 0.85$*, (e) and comparison controller.*

https://doi.org/10.1017/S0263574723001601 Published online by Cambridge University Press

6. Conclusion

In this article, a HIAC scheme is developed for robot manipulators to interact with the second-order unknown environment. An impedance adaptation method with virtual inertia is proposed to make the manipulators have the optimal interaction behavior described by the second-order target impedance model without the need for accurate environment dynamics and acceleration feedback. A hybrid system framework suitable for the second-order environment is proposed to generate a series of intermediate controllers to interpolate between the responses of impedance control and admittance control by adjusting the duty cycle of the switching controller. A mapping of the optimal duty cycle is built to select the optimal intermediate controller to provide the optimal implementation performance for the obtained target impedance model. Simulation and experimental studies on the Franka EMIKA panda robot have verified the effectiveness of the proposed HIAC scheme, and the proposed hybrid system framework shows higher trajectory tracking accuracy than the comparison hybrid controller in the experiment. In practice, robots may need to interact with fast time-varying environments in complex tasks, and free-space/contact phase switching is inevitable during this process. In future work, we will consider improving our scheme to adapt to interactions with fast time-varying environments and integrating the free-space/contact phase switching controller [13] into our framework to deal with the impact and force overshoots. Moreover, we will be committed to combining our hybrid controllers and the advanced adaptive impedance controllers [8, 9] to eliminate the impact of system uncertainties and further improve control performance.

Author contributions. Dexi Ye conceived and designed the study, collected the data, and wrote the manuscript. Yiming Jiang and Hui Zhang analyzed and interpreted the data and wrote the manuscript. Chenguang Yang conceived and designed the study, wrote and revised the manuscript, and supervised the study. All authors have read and approved the final manuscript.

Financial support. This work was supported in part by National Nature Science Foundation of China (NSFC) under Grant U20A20200, Grant 92148204 and Grant 62003136, in part by Guangdong Basic and Applied Basic Research Foundation under Grant 2020B1515120054, in part by Industrial Key Technologies R & D Program of Foshan under Grant 2020001006308 and Grant 2020001006496, and in part by the Open Research Fund from Guangdong Laboratory of Artificial Intelligence and Digital Economy (SZ) (GML-KF-22-14).

Competing interests. The authors declare that the research was conducted in the absence of any commercial or financial relationships that could be construed as a potential conflict of interest.

Ethical approval. None.

References

[1] J. Jiang, L. Yao, Z. Huang, G. Yu, L. Wang and Z. Bi, "The state of the art of search strategies in robotic assembly," *J. Ind. Inf. Integr.* **26**, 100259 (2022).
[2] D. Mukherjee, K. Gupta, L. H. Chang and H. Najjaran, "A survey of robot learning strategies for human-robot collaboration in industrial settings," *Robot. Comput. Integr. Manuf.* **73**, 102231 (2022).
[3] M. H. Raibert and J. J. Craig, "Hybrid position/force control of manipulators," *J. Dyn. Syst. Meas. Control* **103**(2), 126–133 (1981).
[4] N. Hogan, "Impedance Control: An Approach to Manipulation," **In:** 1984 American Control Conference (1984) pp. 304–313.
[5] P. Song, Y. Yu and X. Zhang, "A tutorial survey and comparison of impedance control on robotic manipulation," *Robotica* **37**(5), 801–836 (2019).
[6] J. E. Colgate and N. Hogan, "Robust control of dynamically interacting systems," *Int. J. Control* **48**(1), 65–88 (1988).
[7] S. P. Buerger and N. Hogan, "Complementary stability and loop shaping for improved human–robot interaction," *IEEE Trans. Robot.* **23**(2), 232–244 (2007).
[8] A. Izadbakhsh and S. Khorashadizadeh, "Polynomial-based robust adaptive impedance control of electrically driven robots," *Robotica* **39**(7), 1181–1201 (2021).
[9] A. Izadbakhsh, A. Deylami and S. Khorashadizadeh, "Superiority of q-Chlodowsky operators versus fuzzy systems and neural networks: Application to adaptive impedance control of electrical manipulators," *Expert Syst. Appl.* **209**, 118249 (2022).

https://doi.org/10.1017/S0263574723001601 Published online by Cambridge University Press

[10] A.-N. Sharkawy and P. N. Koustoumpardis, "Human–robot interaction: A review and analysis on variable admittance control, safety, and perspectives," *Machines* **10**(7), 591 (2022).
[11] Z. Jin, D. Qin, A. Liu, W.-a. Zhang and L. Yu, "Model predictive variable impedance control of manipulators for adaptive precision-compliance tradeoff," *IEEE/ASME Trans. Mechatron.* **28**(2), 1174–1186 (2022).
[12] A.-N. Sharkawy, P. N. Koustoumpardis and N. Aspragathos, "A neural network-based approach for variable admittance control in human–robot cooperation: Online adjustment of the virtual inertia," *Intell. Serv. Robot.* **13**(4), 495–519 (2020).
[13] L. Roveda, D. Riva, G. Bucca and D. Piga, "Sensorless optimal switching impact/force controller," *IEEE Access* **9**, 158167–158184 (2021).
[14] L. Roveda, A. A. Shahid, N. Iannacci and D. Piga, "Sensorless optimal interaction control exploiting environment stiffness estimation," *IEEE Trans. Control Syst. Technol.* **30**(1), 218–233 (2022).
[15] L. Roveda, A. Testa, A. A. Shahid, F. Braghin and D. Piga, "Q-Learning-based model predictive variable impedance control for physical human-robot collaboration," *Artif. Intell.* **312**, 103771 (2022).
[16] Y. Li and S. S. Ge, "Impedance learning for robots interacting with unknown environments," *IEEE Trans. Control Syst. Technol.* **22**(4), 1422–1432 (2014).
[17] G. Peng, C. L. P. Chen and C. Yang, "Robust admittance control of optimized robot-environment interaction using reference adaptation," *IEEE Trans. Neural Netw. Learn. Syst.* **34**(9), 5804–5815 (2022).
[18] C. Zeng, C. Yang and Z. Chen, "Bio-inspired robotic impedance adaptation for human-robot collaborative tasks," *Sci. China Inf. Sci.* **63**(7), 170201 (2020).
[19] H. Qiao, S. Zhong, Z. Chen and H. Wang, "Improving performance of robots using human-inspired approaches: A survey," *Sci. China Inf. Sci.* **65**(12), 221201 (2022).
[20] H. Qiao, Y.-X. Wu, S.-L. Zhong, P.-J. Yin and J.-H. Chen, "Brain-inspired intelligent robotics: Theoretical analysis and systematic application," *Mach. Intell. Res.* **20**(1), 1–18 (2023).
[21] F. L. Lewis, D. Vrabie and V. L. Syrmos, *Optimal Control* (John Wiley & Sons, New York, 2012).
[22] F.-Y. Wang, H. Zhang and D. Liu, "Adaptive dynamic programming: An introduction," *IEEE Comput. Intell. Mag.* **4**(2), 39–47 (2009).
[23] Y. Jiang and Z.-P. Jiang, "Computational adaptive optimal control for continuous-time linear systems with completely unknown dynamics," *Automatica* **48**(10), 2699–2704 (2012).
[24] S. S. Ge, Y. Li and C. Wang, "Impedance adaptation for optimal robot–environment interaction," *Int. J. Control* **87**(2), 249–263 (2014).
[25] H. Huang, C. Yang and C. L. P. Chen, "Optimal robot–environment interaction under broad fuzzy neural adaptive control," *IEEE Trans. Cybern.* **51**(7), 3824–3835 (2021).
[26] C. Yang, G. Peng, Y. Li, R. Cui, L. Cheng and Z. Li, "Neural networks enhanced adaptive admittance control of optimized robot–environment interaction," *IEEE Trans. Cybern.* **49**(7), 2568–2579 (2019).
[27] T. Valency and M. Zacksenhouse, "Accuracy/robustness dilemma in impedance control," *J. Dyn. Syst. Meas. Control* **125**(3), 310–319 (2003).
[28] C. Ott, R. Mukherjee and Y. Nakamura, "Unified Impedance and Admittance Control," **In:** *2010 IEEE International Conference on Robotics and Automation* (IEEE, Anchorage, AK, 2010) pp. 554–561.
[29] C. Ott, R. Mukherjee and Y. Nakamura, "A hybrid system framework for unified impedance and admittance control," *J. Intell. Robot. Syst.* **78**(3-4), 359–375 (2015).
[30] A. Formenti, G. Bucca, A. A. Shahid, D. Piga and L. Roveda, "Improved impedance/admittance switching controller for the interaction with a variable stiffness environment," *Complex Eng. Syst.* **2**(3), 12 (2022).
[31] I. Rhee, G. Kang, S. J. Moon, Y. S. Choi and H. R. Choi, "Hybrid impedance and admittance control of robot manipulator with unknown environment," *Intell. Serv. Robot.* **16**, 49–60 (2022).
[32] F. Cavenago, L. Voli and M. Massari, "Adaptive hybrid system framework for unified impedance and admittance control," *J. Intell. Robot. Syst.* **91**(3-4), 569–581 (2018).
[33] J.-J. E. Slotine and W. Li, *Applied Nonlinear Control* (Prentice Hall, Englewood Cliffs, NJ, 1991).
[34] T. Das and R. Mukherjee, "Shared-sensing and control using reversible transducers," *IEEE Trans. Control Syst. Technol.* **17**(1), 242–248 (2009).

Cite this article: D. Ye, C. Yang, Y. Jiang and H. Zhang (2024). "Hybrid impedance and admittance control for optimal robot–environment interaction", Robotica **42**, 510–535. https://doi.org/10.1017/S0263574723001601

https://doi.org/10.1017/S0263574723001601 Published online by Cambridge University Press